Journal of Hazardous Materials 515 (2026) 143238

Contents lists available at ScienceDirect

Journal of Hazardous Materials

journal homepage: www.elsevier.com/locate/jhazmat

Halogenated bisphenol A alternatives inhibit aldo-keto reductase 1C1 and induce metabolic alterations in human adipocytes

Jasmin Kleißen [a], Cornelius Goerdeler [a,1], Alix Sarah Aldehoff [a], Isabel Karkossa [a], Anna Didio [a,b], Johannes Schmidt [c], Stefan Kalkhof [c,d], Jörg Lehmann [c,d], Ulrike Rolle-Kampczyk [a], Marina Grimaldi [e], Patrick Balaguer [e], Maximilian Faissner [f], Christoph Flamm [f], Martin Wabitsch [g,h], John Thomas Heiker [i,j], Kristin Schubert [a,b,*,2], Martin von Bergen [a,h,j,k,*,2]

[a] Department of Molecular Toxicology, Helmholtz-Centre for Environmental Research GmbH (UFZ), Permoserstraße 15, Leipzig 04318, Germany
[b] Cell Biology, Faculty of Environment and Natural Science, Brandenburg University of Technology Cottbus-Senftenberg, Universitätsplatz 1, Senftenberg 01968, Germany
[c] Fraunhofer Institute for Cell Therapy and Immunology IZI, Department of Preclinical Development and Validation, Perlickstraße 1, Leipzig 04103, Germany
[d] Fraunhofer Cluster of Excellence Immune-Mediated Diseases CIMD, Frankfurt/Main, Hannover, Perlickstraße 1, Leipzig 04103, Germany
[e] Institut de Recherche en Cancérologie de Montpellier (IRCM), INSERM, U1194, Université de Montpellier, Institut régional du Cancer de Montepellier (ICM), Parc Euromédecine, 208 Av. des Apothicaires, Montpellier 34090, France
[f] Institute for theoretical chemistry, University of Vienna, Währinger Straße 17, Vienna 1090, Austria
[g] Division of Paediatric Endocrinology and Diabetes, University Hospital for Children and Adolescents Ulm, Eythstraße 24, Ulm 89075, Germany
[h] German Centre for Child and Adolescent Health (DZKJ), Frauensteige 14A, Ulm 89075, Germany
[i] Helmholtz Institute for Metabolic, Obesity and Vascular Research (HI-MAG) of Helmholtz Munich at the University of Leipzig and University Hospital, Philipp-Rosenthal-Straße 27, Leipzig 04103, Germany
[j] Institute of Biochemistry, Faculty of Life Sciences, University of Leipzig, Talstraße 33, Leipzig 04103, Germany
[k] German Centre for Integrative Biodiversity Research (iDiv) Halle-Jena-Leipzig, Puschstraße 4, Leipzig 04103, Germany

Abbreviations: 3PG, 3-phosphoglycerate; AcCoA, AcetylCoA; ACN, Acetonitrile; AGC, Automatic gain control; AKG, Alpha-ketoglutarate; AKR1C1, Aldo-keto reductase 1 C1; Ala, Alanine; Asn, Asparagine; Asp, Aspartate; ATP, Adenosine triphosphate; BPA, Bisphenol A; BPS, Bisphenol S; CAco, Cis-aconitate; Cit, Citrate; DAPI, 4,6-Diamidino-2-Phenylindole, Dihydrochloride; DIA, Data-independent acquisition; DMEM, Dulbecco's Modified Eagle Medium; DMSO, Dimethyl-sulfoxide; EATS, Estrogen, androgen, thyroid, steroidogenesis; ECM, Extracellular matrix; EDC, Endocrine-disrupting chemicals; FC, Fold change; FCS, Fetal calf serum; Frc1, 6BP, Fructose 1,6-bisphosphate; Frc6P, Fructose 6-phosphate; Fum, Fumarate; G3P, Glyceraldehyde 3-phosphate; Glc6P, Glucose 6-phosphate; Gln, Glutamine; GLUD1, Glutamate-dehydrogenase 1; Glut, Glutamate; Gro3P, Glycerol 3-phosphate; HCD, Higher-energy collisional dissociation; HFD, High-fat diet; HPLC, Nano high performance liquid chromatography; KEGG, Kyoto Encyclopedia of Genes and Genomes; Lac, Lactate; LBP, Ligand-binding pocket; LC-MS/MS, Liquid chromatography-tandem mass spectrometry; MaCoA, Malonyl-CoA; Mal, Malate; MCP-1, Monocyte chemotactic protein-1; MDC, Metabolism-disrupting chemicals; MINCH, Monoisononylcyclohexane-1,2-dicarboxylic acid ester; MM-GBSA, Molecular mechanics-based generalized Born surface area calculations; MM-PBSA, Molecular mechanics-based generalized Poisson-Boltzmann surface area calculations; NAD +, Nicotinamide adenine dinucleotide; NADPH, Nicotinamide adenine dinucleotide phosphate; NanoDSF, Nano differential scanning fluorescence; NMDR, NIH Common Fund's National Metabolomics Data Repository; OAA, Oxaloacetate; PBS, Phosphate-buffered saline; PCA, Principal component analysis; PEP, Phosphoenolpyruvate; PMVK, Phosphomevalonate kinase; PPARγ, Peroxisome proliferator-activated receptor γ; PPP, Pentose phosphate pathway; PSAT1, Phosphoserine aminotransferase 1; Pyr, Pyruvate; Ribose5P, Ribose 5-phosphate; Ribu5P, Ribulose 5-phosphate; RMSD, Root-mean-square deviation; Sedu7P, Sedoheptulose 7-phosphate; SGBS, Simpson-Golabi-Behmel syndrome; SP3 beads, SpeedBeads™ magnetic carboxylate modified particles; Suc, Succinate; TBBPA, Tetrabromobisphenol A; TBBPS, Tetrabromobisphenol S; TCA, Tricarboxylic acid; TCBPA, Tetrachlororbisphenol A; TCBPS, Tetrachlororbisphenol S; TEAB, Tetraethylammonium bromide; Tm, Melting point; TMT, Tandem mass tag; TPP, Thermal proteome profiling; ΔTm, Difference in melting point.

* Correspondence to: Department of Molecular Toxicology, Helmholtz Centre for Environmental Research, Permoserstraße 15, Leipzig 04318, Germany.
E-mail addresses: jasmin.kleissen@ufz.de (J. Kleißen), Cornelius.Goerdeler@bfr.bund.de (C. Goerdeler), alix-sarah.aldehoff@ufz.de (A.S. Aldehoff), isabel.karkossa@yahoo.com (I. Karkossa), anna.didio@b-tu.de (A. Didio), johannes.schmidt.hro@gmail.com (J. Schmidt), stefan.kalkhof@izi.fraunhofer.de (S. Kalkhof), joerg.lehmann@izi.fraunhofer.de (J. Lehmann), ulrike.rolle-kampczyk@ufz.de (U. Rolle-Kampczyk), marina.dilillo-grimaldi@inserm.fr (M. Grimaldi), patrick.balaguer@inserm.fr (P. Balaguer), maximilian.faissner@univie.ac.at (M. Faissner), xtof@tbi.univie.ac.at (C. Flamm), Martin.Wabitsch@uniklinik-ulm.de (M. Wabitsch), john.heiker@helmholtz-munich.de (J.T. Heiker), kristin.schubert@b-tu.de (K. Schubert), martin.vonbergen@ufz.de (M. von Bergen).
[1] German Federal Institute of Risk Assessment (BfR), Max-Dohrn-Straße 8-10, 10589 Berlin, Germany (current address)
[2] Authors contributed equally

https://doi.org/10.1016/j.jhazmat.2026.143238
Received 26 May 2026; Received in revised form 3 August 2026; Accepted 6 August 2026
Available online 8 August 2026

HIGHLIGHTS

- Halogenated BPA substitutes induce triglyceride accumulation in human adipocytes.
- Integrated proteomics and metabolomics assays uncover metabolic effects.
- TPP identifies novel protein targets of halogenated BPA analogues.
- Targeted enzyme inhibition validates functional compound-protein links.
- Multiple bisphenols inhibit AKR1C1's enzymatic activity.

GRAPHICAL ABSTRACT

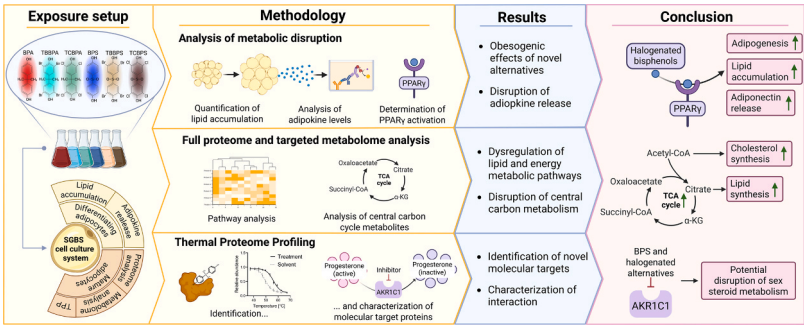

ARTICLE INFO

Keywords:
BPA
Halogenated BPA alternatives
Adipocytes
Metabolic disruption
Thermal proteome profiling
TCA cycle
Steroid metabolism

ABSTRACT

Bisphenol A (BPA) is a widely used plastic monomer with well-established endocrine-disrupting properties and emerging evidence for metabolism-disrupting effects. Following regulatory restrictions, structurally modified alternatives, including halogenated derivatives, have been introduced, but information on their metabolic effects remains scarce. Hence, we analyzed proteomic and metabolomic responses in SGBS human adipocytes after exposure to BPA and five analogues (TBBPA, TCBPA, BPS, TBBPS, and TCBPS), including environmentally relevant concentrations of 10 nM. Intracellular target proteins were identified using thermal proteome profiling (TPP). All tested alternatives significantly increased intracellular triglyceride levels, indicating adipogenic potential. Proteomic and metabolomic analyses revealed alterations in lipid and energy metabolism and the central carbon cycle. TPP identified protein targets within steroid hormone pathways, fatty acid, central carbon, and amino acid metabolism, which were confirmed by nano differential scanning fluorimetry. Among these, AKR1C1 showed strong binding interactions with the tested bisphenols, resulting in reduced enzymatic activity. Pharmacological inhibition of AKR1C1 induced metabolic changes resembling those caused by BPS and its halogenated derivates. Overall, these findings identify AKR1C1 as a potential molecular target of halogenated bisphenols and demonstrate that these compounds disrupt adipocyte metabolism highlighting the importance of mechanistic data of chemical risk assessment.

1. Introduction

The global obesity pandemic has accelerated rapidly, with prevalence rates nearly tripling over the past 50 years [1]. Approximately 890 million adults and 160 million children worldwide are classified as obese [1]. While a high-calorie diet, lack of physical activity, and genetic predisposition remain key factors in the development of obesity, they may not fully explain the swift global rise in obesity rates [2]. This has prompted growing interest in environmental factors that may contribute to metabolic dysregulation.

Among these, metabolism-disrupting chemicals (MDCs) are increasingly recognized as potential drivers of obesity and associated metabolic disorders [3,4]. MDCs represent a functionally defined subgroup of endocrine-disrupting chemicals (EDCs) that interfere with metabolic homeostasis through diverse molecular mechanisms. Their widespread use in consumer products leads to ubiquitous human exposure [5].

Importantly, the effects of MDCs are not restricted to classical EATS (estrogen, androgen, thyroid, steroidogenesis) pathways. Instead, MDCs can act through non-EATS modalities, including the modulation of nuclear receptors such as the peroxisome proliferator-activated receptor γ (PPARγ), disruption of mitochondrial function, interference with insulin and glucose signaling, induction of oxidative stress, and alterations in lipid metabolism and adipocyte differentiation [3,5,6].

In this context, adipose tissue has emerged as a central target organ for MDC action [3]. Beyond its role as a triglyceride storage site, adipose tissue functions as a highly active endocrine organ that integrates systemic signals and secretes adipokines and cytokines with widespread metabolic effects [7]. Disruption of adipose tissue signaling by MDCs can impair key metabolic pathways, including those involved in energy and lipid metabolism, adipocyte differentiation, and insulin signaling [8].

One of the most extensively studied metabolic endocrine-disrupting chemicals associated with adipose tissue dysfunction and obesity is bisphenol A (BPA). Its estimated global production volume is 10 million tons per year [9]. The monomer is used in the manufacturing of polycarbonate plastics and is found in the epoxy resin coating of food packaging and drinking cans, as precursors for flame retardants, in medical items and thermal paper recipes, among others [10]. Its wide spread use results in ubiquitous human exposure and widespread detectability in biological samples [11,12].

BPA has been linked to a range of adverse health outcomes, including reproductive, neurological and developmental dysfunctions [13]. More recently, BPA's potential to disrupt metabolic processes has garnered increasing attention. Associations between BPA levels in urine or blood and obesity, as well as related comorbidities, have been reported [14–17]. Furthermore, BPA plasma levels correlate with markers of the metabolic syndrome and insulin resistance [18].

In previous studies BPA has shown to induce oxidative stress in a variety of cell types and tissues [19–21] thereby impairing mitochondrial function, resulting in alterations in energy metabolism, mitochondrial DNA integrity, mitophagy, and apoptosis [22].

In vitro, BPA has been shown to induce several metabolic alterations in murine and human adipocyte models, including increased lipid accumulation, enhanced adipocyte differentiation, altered adipokine signaling, changes in insulin sensitivity and dysregulated expression of

genes involved in lipid metabolism and adipogenesis [23–27]. However, the underlying molecular mechanisms driving these effects remain poorly understood. Some studies describe an agonistic effect of BPA on PPARγ [23], a key regulator of adipocyte function [28]. In contrast, other studies failed to detect a direct interaction between BPA and PPARγ [29,30] or even reported antagonistic effects [31]. Additionally, BPA has also shown to induce the expression of genes involved in early adipogenesis and lipogenesis including but not limited to PPARγ [32,33]. These varying results, likely due to differences in tested concentrations and model systems, underscore the need for further investigation into the molecular mechanisms underlying BPA-mediated metabolic disruption.

Due to the wide range of adverse health effects associated with BPA, the compound was classified as a 'substance of very high concern' by the European Commission under European chemical legislation [34]. Following restrictions on BPA, structurally similar compounds such as bisphenol S (BPS) have emerged as common replacements in consumer products. However, growing evidence indicates that BPS exerts metabolic disrupting effects comparable to those of BPA, suggesting shared modes of action [31,35]. In addition to BPS, other BPA-related compounds, including halogenated analogues like tetrabromobisphenol A (TBBPA) and tetrachlorobisphenol A (TCBPA), are employed in industrial applications, most notably as flame retardants. Despite differing functional applications, these compounds raise similar concerns regarding their potential adverse health effects [36–38]. With a production volume of $>$ 100,000 t/year, TBBPA is the most widely produced brominated flame retardant [36]. Dufour et al. [39] were able to detect TBBPA in the serum of 31% of 274 tested adult individuals in Belgium. Halogenated derivatives of BPS, such as tetrabromobisphenol S (TBBPS) and tetrachlorobisphenol S (TCBPS), have also been introduced as replacements for TBBPA in response to rising concerns [36]. Specifically, TBBPS is a common substitute for TBBPA and with rising exposure levels being detected in environmental matrices, including water, soil, and waste water [40–42]. TBBPS was detected in 89.5% of human blood samples with an average concentration of 0.593 ng/mL [43]. Interestingly, TBBPA and TCBPA are both able to bind and activate PPARγ and have shown an adipogenic effect in both 3T3-L1 mouse adipocytes and zebrafish [30,44]. Comparable effects were demonstrated for TBBPS in 3T3-L1 mouse adipocytes [45]. However, data on the metabolism-disrupting properties of these compounds remain limited.

To systematically investigate the influence of halogenation on bisphenol activity and to identify both shared and compound-specific molecular mechanisms, this study included BPA, BPS, and their brominated and chlorinated analogues TBBPA, TCBPA, TBBPS, and TCBPS. Using the human preadipocytes of the Simpson-Golabi-Behmel syndrome (SGBS) cell strain as a cell culture model, the adipogenic effects of these compounds were investigated. The compounds were analyzed using lipid accumulation assays during adipogenesis as an initial screening method to assess their adipogenic potential. Specifically, the setup not including rosiglitazone as a PPARγ agonist aims to show their potential to interact with this master adipogenesis regulator. Complementary, bisphenol-induced PPARγ activation was measured. To determine the effects of the chemicals on adult adipocytes as the main cell type in adipose tissue, global proteomics and targeted metabolomics were utilized. To identify molecular targets beyond PPARγ, thermal proteome profiling (TPP) was applied [46,47], resulting in the identification of both shared and compound-specific protein targets.

The concentrations for the adipokine, proteomic and metabolomic analyses (10 nM and 10 μM) were selected to represent both an environmentally relevant exposure level, as BPA has been detected in multiple human matrices in a range between 5 and 30 nM [48–50], and an effect-driven concentration of 10 μM. The same concentrations were applied to all investigated bisphenols to ensure direct comparability between compounds and across experimental platforms, including TPP. For TPP, 10 μM was additionally chosen based on methodological considerations and in accordance with Aldehoff et al. [51], where this concentration enabled robust target identification.

Based on TPP candidates, selected proteins were further examined using selective inhibitors, while additionally investigating candidate enzymes by molecular docking and molecular dynamics simulations to assess plausible bisphenol binding modes. These analyses were then used to characterize the downstream effects on the proteome, enzyme activity and metabolic processes.

The objective of this study was to comprehensively characterize the metabolic effects of halogenated bisphenols in human adipocytes and to elucidate their underlying molecular mechanisms. Specifically, this study aimed to determine whether halogenated bisphenols exhibit adipogenic properties in human adipocytes, whether the emerging BPS derivatives TBBPS and TCBPS directly interact with human PPARγ, and how these compounds influence cellular metabolism, with particular emphasis on central carbon and lipid metabolic pathways. Furthermore, the study investigated how halogenation alters the metabolic activity of BPA and BPS and sought to identify protein targets and molecular interaction partners of these compounds within the proteome of human adipocytes using TPP.

2. Methods

2.1. SGBS cell culture

Human SGBS preadipocytes were selected as the experimental model because differentiated SGBS adipocytes closely resemble primary human adipocytes from healthy donors with respect to morphology, adipogenic capacity, insulin responsiveness, and adipokine secretion [39]. Moreover, SGBS cells are a well-established and widely used human *in vitro* model for investigating adipogenesis, adipocyte metabolism, and the effects of metabolism-disrupting chemicals [31,52,53]. Compared with primary adipocytes, SGBS cells provide a homogeneous and reproducible model system with substantially lower donor-to-donor variability, thereby improving the comparability of experimental results across multiple analytical platforms [51]. In addition, TPP requires large amounts of cellular protein for lysate preparation, which would be difficult to obtain from primary human adipocytes in a reproducible and practical manner. The use of the SGBS cell line therefore provided both a biologically relevant human adipocyte model and the experimental feasibility required for the comprehensive proteomic analyses performed in this study.

SGBS cell culture handling is described elsewhere [54]. In brief, cells were maintained at 37 °C with 5% CO_2 and 95% humidity. Cells were grown to confluence in Dulbecco's Modified Eagle Medium (DMEM)/F12 medium supplemented with 17 μM pantothenate, 33 μM biotin, 1 nM penicillin, 1 nM streptomycin and 10% fetal calf serum (FCS) (growth medium). Differentiation was induced (day 0) by changing to an FCS-free basal medium. The cells were first washed with pure DMEM/F12 medium and subsequently treated with FCS-free basal medium containing 0.01 mg/mL transferrin, 20 nM insulin, 100 nM cortisone, and 0.2 nM triiodothyronine. Additionally, during the first 4 days of differentiation the medium was supplemented with 25 nM dexamethasone, 500 μM 3-isobutyl−1-methylxanthine and 2 μM rosiglitazone (initiation QD medium). These three supplements were omitted during the following 8 days of differentiation (maintenance 3FC medium).

2.2. DAPI and Nile Red staining of SGBS cells

To assess the effect of bisphenols during adipogenesis on cytotoxicity and lipid accumulation, the differentiation media (both initiation QD and maintenance 3FC medium) was supplemented with bisphenols in concentrations ranging from 1 nM to 100 μM bisphenols. Usually, SGBS adipocytes are differentiated with the addition of rosiglitazone in the differentiation medium during the first 4 days. To determine a potential interaction with the main regulator of adipogeneses, PPARγ, the assay

was performed under two conditions: with and without 2 μM rosiglitazone during the first 4 days of differentiation. The results from the experimental setup including rosiglitazone can be found in the supplements (Sup. Fig. 1).

Cytotoxicity was evaluated by quantifying the cells' DNA content using 4,6-diamidino−2-phenylindole (DAPI) staining, while triglyceride accumulation in lipid droplets of differentiated adipocytes was simultaneously assessed using Nile Red staining as described by Aldridge et al. [55]. In brief, SGBS cells were grown to confluence in 96-well plates in growth medium, as described in Section 2.1. After washing cells with pure DMEM/F12 medium, cells were treated with differentiation medium (QD and 3FC) supplemented with bisphenols for 12 days with medium changes every 48 h. For control condition, cells were treated with differentiation medium containing 0.01% dimethyl-sulfoxide (DMSO) for 12 days, either in the presence or absence of rosiglitazone, respectively. Experiments were performed in quadruplicate. On day 12, cells were washed three times with phosphate-buffered saline (PBS, Biowest, Nuaillé, France) and fixated with 4% paraformaldehyde in PBS for 1 h at room temperature. Afterwards, cells were washed with PBS and stained with 100 μL staining solution per well containing 0.1% saponin (Sigma Aldrich, St. Louis, MO, USA), 1 μg/mL DAPI (Thermo Fisher Scientific, Waltham, MA, USA) and 1 μg/mL Nile Red (Sigma Aldrich) for 30 min at room temperature in the dark. Cells were washed twice with PBS before fluorescence was measured on cells with 200 μL PBS at Ex 360/Em 480 for DAPI and Ex 485/Em 530 for Nile Red in a 5 × 5 spot pattern. The ratio of Nile Red to DAPI fluorescence intensity was calculated to normalize for differences in cell number between wells. Fluorescence images were acquired using a fluorescence microscope (BZ-X810, Keyence, Osaka, Japan) following Nile Red and DAPI staining.

2.3. Reporter cell line assay

The generation of HGLN and HGLN-GAL4-PPARγ reporter cell lines was performed as previously described [56,57]. Briefly, reporter cells were seeded at a density of 20,000 cells per well in white, opaque 96-well tissue culture plates and maintained in phenol-red–free DMEM supplemented with 5% dextran-coated, charcoal-treated FCS. After 24 h, the culture medium was replaced with DMEM containing the test compounds. Sixteen hours post-exposure, the medium was replaced with fresh medium containing 0.3 mM luciferin. Luminescence was then measured in intact, living cells for 2 s using a Microbeta Wallac luminometer (PerkinElmer, Waltham, MA, USA).

2.4. Adipokine release

SGBS cells were cultivated in 24-well plates and differentiated for 12 days. The 3FC medium of the mature adipocytes was then supplemented with 10 nM or 10 μM of the different bisphenols for 24 h, 4 days, or 8 days, respectively. The release of adipokines leptin, adiponectin and monocyte chemotactic protein−1 (MCP−1) of SGBS cells during exposure to bisphenols was quantified in the cell culture supernatant of mature SGBS adipocytes. All samples were tested using the DuoSet™ ELISA kits from Bio-techne/R&D Systems (Minneapolis, MN, USA). Experiments were performed in quadruplicate and according to the manufacturer's instructions.

2.5. Protein harvest and proteomics LC-MS/MS analysis

SGBS cells were cultivated in 24-well plates and differentiated for 12 days. The 3FC medium of the mature adipocytes was then supplemented with 10 nM and 10 μM of the different bisphenols and the inhibitor for the most prominent target protein identified in the TPP (AKR1C1: 3-bromo−5-phenylsalicylic acid; Sigma Aldrich). Controls included 2 μM rosiglitazone (as a PPARγ agonist), 10 μM GW9662 (as a PPARγ antagonist), and a 0.1% (v/v) DMSO vehicle control. Experiments were performed in quadruplicate. After 24 h, 4 days and 8 days, respectively, supernatants were collected for adipokine quantification (see Section 2.4) and cells were washed with ice cold PBS. After discarding PBS, 100 μL ice-cold lysis buffer per well was added (150 mM NaCl, 0.1% sodium dodecyl sulphate, 0.5% sodium deoxycholate, 50 mM Tris-HCL, 1% Triton X−100, and cOmplete™ Protease Inhibitor Cocktail (Roche, Basel, Switzerland). Cells were harvested using a cell scraper and incubated for 1 h on ice. Samples were then centrifuged at 16,100x*g* for 15 min at 4 °C. Lysates were transferred to new tubes to discard cell debris. Protein concentration was determined using the DC assay (Bio Rad, Hercules, CA, USA) according to manufacturer's instructions.

Cell lysates were prepared using Sera-Mag SP3 beads (SpeedBeads™ magnetic carboxylate-modified particles (SP3 beads; GE Healthcare, Germany). For each sample, 2 μg beads were washed in 100 μL water. Tubes were placed on magnetic rack and incubated for 2 min. Water was discarded and washing step was repeated. Washed beads were transferred into a 96-well plate, placed on a magnetic rack and supernatant was discarded. A volume corresponding to 10 μg of protein at the lowest incubation temperature was taken from each sample and brought to an equal volume of 70 μL using 100 mM tetraethylammonium bromide (TEAB). Proteins were reduced with 5 μL 200 mM tris(2-carboxyethyl) phosphine (55 °C, 1 h, 550 rpm) and alkylated with 5 μL 375 mM indole−3-acetic acid (room temperature, 550 rpm, protected from light). To force protein binding, 90 μL acetonitrile (ACN) was added, each sample was transferred to the washed beads in the 96-well plate and incubated for 8 min off the magnetic rack. Afterwards, the plate was put back on the rack and supernatant was discarded. For protein clean-up 200 μL of 70% (v/v) EtOH in water was added to each well. The plate was placed on the magnetic rack for 30 s and the supernatant was discarded. This step was repeated twice with 70% (v/v) EtOH and once with 200 μL 100% ACN. ACN was removed and beads were dried before adding trypsin (Promega, Madison, WI, USA, 1:50 enzyme to protein, 37 °C, 16 h). Afterwards, for peptide clean-up, 150 μL 100% ACN was added to each well to support peptide binding and samples were incubated for 8 min off the magnetic rack. The plate was then placed on the magnetic rack for 2 min, the supernatant was discarded, and samples were washed with 200 μL 100% ACN. Peptides were eluted twice with 50 μL 2% (v/v) DMSO in water using sonication and combined in tubes. The tubes were placed on the magnetic rack for 2 min and the supernatant was recovered. Samples were then evaporated in a vacuum centrifuge, reconstituted in 0.1% (v/v) FA and analyzed using liquid chromatography-tandem mass spectrometry (LC-MS/MS).

Samples were loaded into the autosampler of a Vanquish Neo UHPLC system (Thermo Fisher Scientific) coupled to an Orbitrap Astral mass spectrometer (Thermo Fisher Scientific). For each run, 400 ng of peptides (0.4 μL injection volume) were first loaded onto a PepMap™ Neo Trap column (0.5 cm × 300 μm, 5 μm, 100 Å, C18; Thermo Fisher Scientific) and subsequently separated on an analytical column (AUR3–25075C18-XT, 25 cm × 75 μm, 1.8 μm, 120 Å, C18; IonOpticks) maintained at 50 °C.

Peptides were eluted using a 30-min three-step gradient at a flow rate of 0.5 μL/min. Mobile phase A consisted of 0.1% formic acid (FA) in water and mobile phase B of 80% ACN with 0.1% FA. The gradient increased from 4% to 48% B as follows: 0.40–16.5 min, 8–25% B; 16.5–22.5 min, 25–35% B; and 22.5–26.0 min, 35–48% B. Column washing and re-equilibration were performed at 0.5 μL/min, including a high-organic wash step at 99% B from 26.0 to 30.0 min.

Electrospray ionization was operated in positive-ion mode at 1.5 kV, with the ion transfer tube temperature set to 280 °C. The Orbitrap Astral was operated in data-independent acquisition (DIA) mode. Full MS scans were acquired at a resolution of 240,000 over an m/z range of 380–980, with one MS1 scan every 0.6 s. DIA acquisition covered the same m/z range using automatically generated, non-overlapping 2 m/z isolation windows (299 total). MS2 spectra were acquired using higher-energy collisional dissociation (HCD) at 25% normalized collision energy and detected in the Astral analyzer over an m/z range of 150–2000. The

maximum injection time was set to 3 ms, and the automatic gain control (AGC) target was 500% for both MS1 and MS2 scans.

A spectral library was generated *in silico* using DIA-NN (version 2.2.0) with default settings, based on the UniProtKB *Homo sapiens* reference proteome (reviewed entries; downloaded 28 February 2025, 20,402 entries). Raw DIA data were processed in DIA-NN using default parameters. Downstream data analysis, including filtering, median normalization, variance stabilization, and missing value imputation, was performed using the proteomicsr R package [58]. Proteins identified in at least 3 out of 4 biological replicates were considered reliably identified. Variance stabilization was applied prior to statistical analysis. Missing values were imputed only for proteins that were consistently absent in one condition (4/4 replicates missing) while being reliably detected in the comparison group (at least 3/4 replicates identified; $q = 0.01$). Differential protein abundance was assessed using Students' *t*-tests followed by Benjamini-Hochberg correction for multiple comparisons. Significantly altered proteins (adjusted p-value ≤ 0.05) were used for pathway enrichment using the Kyoto Encyclopedia of Genes and Genomes (KEGG) and REACTOME databases within the framework of proteomicsr R package. Benjamini-Hochberg adjusted p-values and z-scores were used for visualization (data sheets provided in the Supplemental Materials). Data are available via ProteomeXchange with identifier PXD078145.

2.6. Extraction and analysis of central carbon metabolites using targeted mass spectrometry

Metabolites of the central carbon metabolism were analyzed following bisphenol exposure. SGBS cells were seeded into 12-well plates and differentiated for 12 days to mature adipocytes, followed by exposure to the six different bisphenols (10 nM and 10 μM) for 24 h and 8 days, respectively. The culture medium was replaced every 48 h. Metabolites were extracted using a MeOH/chloroform/water (1:1:1) extraction. After removing the culture medium, cells were washed twice with 2 × 1 mL ice-cold 0.9% NaCl. The NaCl was removed and metabolism was quenched by adding 400 μL MeOH (−20 °C) to each well, followed by 400 μL ice-cold H_2O. Then, cells were harvested using a cell scraper and transferred into a 2 mL tube with 400 μL chloroform (−20 °C). The extraction mixtures were shaken at 1400 rpm and 4 °C for 20 min. Afterwards the tubes were centrifuged at 16,000x*g* and 4 °C for 5 min. 300 μL of the polar phase were collected, transferred to a new tube and evaporated to dryness. The metabolite pellets were stored at −20 °C until further analysis and subsequently reconstituted in 100 μL water prior to measurement.

Extracted intracellular central carbon metabolites were analyzed by LC-MS/MS following a modified protocol based on Buescher et al. [59] and published in Goerdeler et al. [52]. Briefly, samples were analyzed using an LC-MS/MS setup consisting of an Agilent 1290 Infinity II UPLC system (Agilent Technologies, Santa Clara, CA, USA) for chromatographic separation, coupled to a QTRAP 6500 + system (AB Sciex, Framingham, MA, USA) for mass spectrometric detection. The mass spectrometer was operated under the following conditions: curtain gas at 45 psig, IonSpray voltage ± 4.5 kV, source temperature 470 °C, Ion Source Gas 1 at 50 psig, and Ion Source Gas 2 at 50 psig, using negative ionization mode. For analysis, 10 μL of each resuspended sample were injected onto an XSelect HSS T3 XP column (2.1 × 150 mm, 2.5 μm, 100 Å; Waters, Milford, MA, USA) equipped with an XP VanGuard cartridge (HSS T3, 2.1 × 5 mm, 2.5 μm; Waters). Chromatographic separation was carried out using a non-linear gradient at flow rates between 0.4 and 0.15 mL/min. The gradient increased stepwise from 0% to 53% B over 0–22.5 min, followed by a return to 100% A and re-equilibration until 33 min. The mobile phase A consisted of 10 mM tributylamine, 10 mM acetic acid, 5% MeOH, and 2% 2-propanol (pH 7.2), while the mobile phase B was 100% 2-propanol. The autosampler temperature was maintained at 8 °C, and the column oven was set to 40 °C. Data acquisition and processing were performed using Analyst and Sciex OS (version 1.6.1.29803). Data is available via NIH Common Fund's National Metabolomics Data Repository (NMDR), study ID ST004842.

2.7. Thermal proteome profiling: protein digest, TMT labeling and HPLC-MS/MS measurement

Thermal Proteome Profiling was performed in cell lysates rather than intact cells to maximize proteome coverage and facilitate the identification of direct protein-compound interactions independent of cellular uptake or intracellular distribution. While this approach increases sensitivity for target discovery, it does not account for physiological factors such as membrane permeability or subcellular compartmentalization [60].

TPP protocol was performed according to Savitski et al. [46]. SGBS cells were cultured and differentiated using 150 mm cell culture dishes with one plate being used per replicate. The experiment was performed in quadruplicate. On day 12 of adipogenesis cells were harvested using cell scrapers in 2 mL PBS supplemented with protease inhibitor per plate. Harvested cells were immediately snap frozen in liquid nitrogen and a freeze-thaw cycle was repeated twice to lyse cells. Lysates were thawed and centrifuged at 16,100x*g* for 20 min at 4 °C. The supernatant was transferred to a new tube to remove cell debris and fat. Protein concentration was determined using the Pierce BCA assay (Thermo Fisher Scientific) according to the manufacturer's instructions. Lysates were diluted 1:1 with PBS, supplemented with protease inhibitor and normalized to a uniform protein concentration (0.67 μg/mL). Lysates were incubated with 10 μM of bisphenols for 10 min at room temperature. Vehicle controls were treated with 0.01% DMSO, corresponding to the final solvent concentration in treated samples. The concentration of 10 μM was chosen in parallel to Aldehoff et al. [51]. After incubation, each replicate was divided into 10 aliquots (100 μL each) and a temperature gradient was applied (37.1, 40.9, 44.1, 47.1, 49.7, 53.2, 56.2, 59.1, 62.4, 67.2 °C) for 3 min using a PCR cycler. Samples were afterwards incubated for 3 min at room temperature before being immediately snap frozen in liquid nitrogen. Samples were centrifuged at 16.100x*g* for 30 min at 4 °C to remove denatured proteins. The fraction of non-denatured proteins in the supernatant was transferred to new tubes.

The applied protein clean-up and digest protocol is described in Section 2.5. After the aforementioned tryptic digest, tandem mass tag (TMT)-labeling was performed as follows: TMT label (Thermo Fisher Scientific) was dissolved in ACN and samples were labelled at a 3:1 label to protein ratio for 1 h at room temperature. Labeling was quenched using 1 μL 5% hydroxylamine in 100 mM TEAB (v/v) and the samples were incubated for 15 min at room temperature. To force peptide binding to the beads 150 μL ACN were added (ACN ≥ 95% (v/v)) and incubated for 8 min at room temperature off the magnetic rack before combining all samples of one replicate with the range of incubation temperatures in one tube. Tubes were then placed on the magnetic rack for 2 min, supernatant was discarded and beads were washed with 100% ACN before eluting twice in 50 μL 2% DMSO in water (v/v), sonicating the samples for 1 min before incubating the eluate on the magnet rack for 2 min. Supernatant was recovered, vacuum-dried and reconstituted in 40 μL ddH_2O. Tubes were placed on magnetic rack for 2 min to gather remaining beads before moving the supernatant into MS vials and acidifying samples to 0.1% (v/v) FA.

Vials were placed into the autosampler of an LC-MS/MS set up with a nano high performance liquid chromatography (HPLC) (Ultimate 3000 RSLCnano, Dionex, Thermo Fisher Scientific) system coupled via a TriVersa Nano Mate (Advion, Ithaka, NY, USA) source in LC chip coupling mode to an Q Exactive™ HF mass spectrometer (Thermo Fisher Scientific). 5 μL of sample were injected and first trapped on a reversed-phase trapping column (Acclaim PepMap 100 C18, 2 μm, 75 μm x 5 cm, nanoViper, Thermo Fischer Scientific) at 4% mobile phase B (80% ACN in water with 0.08% FA) and 96% mobile phase A (nanopure water with

0.1% FA) at a flow rate of 0.3 µl/min, before being separated on an analytical reverse-phase column (Acclaim PepMap 100 C18, nanoViper, 3 µm, 75 µm x 25 cm, Thermo Fisher Scientific). Samples were eluted over a 180 min two-step gradient starting at 4% and ending at 50% of mobile phase B. Separated peptides were analyzed using the Q Exactive mass spectrometer with MS1 scans acquired at a resolution of 120,000 over an *m/z* range of 350–1550. The top 15 precursor ions were selected for MS/MS analysis using a quadrupole isolation window of 0.7 *m/z*, and MS2 spectra were acquired at a resolution of 60,000. The dynamic exclusion was set to 45 s. The MS raw files were processed using ProteomeDiscoverer (version 2.5.0.400) and the database search was performed using the UniprotKB/Swissprot reference proteome of *Homo sapiens* (downloaded on 17 July 2023, 82,158 entries). Data are available via ProteomeXchange with identifier PXD077754.

2.8. Candidate selection from thermal proteome profiling

Candidate search was performed as described in Franken et al. [47]. From the resulting protein abundances, fold changes (FC) relative to the lowest incubation temperature (37.1 °C) were calculated for each condition and replicate. These FCs were analyzed using the R (v. 4.3.0) package TPP (version 3.32.0, [61]) for normalization of protein abundance, melting curve fitting, and melting point identification. The temperature range workflow of the package was used. Normalization was performed as described in Savitski et al. [46]. Melting curves were fitted over the normalized FC of all proteins to determine the melting point of each protein (the temperature at which 50% of the protein precipitated), R^2 (goodness of fit of sigmoidal curve over FC), slope at its steepest point (inflection point of the curve) and plateau (given by the melting curves lower horizontal asymptote). The compound-induced change in protein thermal stability was determined by calculating the melting point difference between vehicle- and compound treated proteins: $T_{m\Delta} = T_{m(treatment)} - T_{m(vehicle)}$. The Student's T test was used to determine the significance of melting point difference between vehicle and treatment. The following filtering criteria were used to ensure the reproducibility and quality of the selected candidate proteins (3 out of 4 replicates per experiment had to pass these criteria): reliable identification (1st), R^2 of > 0.9 (2nd), slope of < -0.06 (3rd), melting point shift in same direction (4th), significant difference in melting points between vehicle and bisphenol treatment (5th) and passing a visual inspection of the fitted melting curves (6th).

2.9. TPP candidate analysis with nanoDSF

A selection of candidate bisphenol-interacting proteins identified in the TPP screening was purchased as recombinant human proteins, all expressed in *Escherichia coli*: AKR1C1 (Bio-techne/R&D systems), glutamate-dehydrogenase 1 (GLUD1; MedChemExpress, Monmouth Junction, NY, USA), phosphoserine aminotransferase 1 (PSAT1; C-terminal 6x His-tagged; R&D Systems), phosphomevalonate kinase (PMVK; C-terminal 6x His-tagged; biomol, Hamburg, Germany). The melting points of the proteins were analyzed by nano differential scanning fluorimetry (nanoDSF) using a Prometheus NT.48 instrument (NanoTemper, Munich, Germany). Optimal substrate concentrations were determined in a trial experiment (data not shown). The concentrations for these trial experiments were based on reported K_m values from the literature. The resulting concentrations are as follows:

- AKR1C1: 265 µM progesterone, 2.65 mM nicotinamide adenine dinucleotide phosphate (NADPH)
- GLUD1: 344 µM L-glutamate, 3.44 mM nicotinamide adenine dinucleotide (NAD+)
- PSAT1: 240 µM L-glutamate, 400 µM 3-phosphooxypyruvate, 250 µM pyridoxal−5'-phosphate
- PMVK: 250 µM (R)−5-phosphomevalonate, 2.5 mM adenosine triphosphate (ATP)

The proteins and substrates were dissolved and/or diluted in the respective protein buffers as follows: AKR1C1, 50 mM tris and 500 mM NaCl; GLUD1, 50 mM tris-HCl, 200 mM NaCl and 20% glycerol; ECH1 ddH_2O; PSAT1, 50 mM tris and 16 mM ammonium acetate and PMVK, ddH_2O. Progesterone (Sigma Aldrich) was dissolved in ethanol, L-glutamate (Sigma Aldrich), (R)−5-phospho-mevalonate (Sigma Aldrich) and ATP (Sigma Aldrich) were solved in PBS. The reactions were carried out in Prometheus High Sensitivity Capillaries (Nanotemper) with 1 µg protein per capillary. Equal concentration of solvent was maintained across all experimental conditions. The optimal bisphenol concentration for the nanoDSF experiments was determined in a test run using AKR1C1 and different concentrations of BPA, TBBPA and BPS (Sup. Fig. 2). A concentration of 100 µM yielded the most robust and reproducible results and was therefore used for all subsequent experiments. Melting curves for each bisphenol were determined in presence and absence of natural substrate and cofactor.

2.10. In silico modelling of bisphenol binding to AKR1C1

Human AKR1C1 lends itself well to *in silico* analysis. It is a monomeric enzyme [62] comprising of 323 amino acid residues (~36.8 kDa), and multiple experimental structures are available for the corresponding UniProt entry Q04828 [63–65]. These include several high-resolution structures co-crystallized with NADP + and either steroid ligands or small-molecule inhibitors. Among the available human AKR1C1 structures, PDB entry 3C3U was selected for docking and molecular dynamics (MD) studies [64]. It represents a wild-type, high-resolution ternary complex with bound NADP + and the inhibitor 3,5-dichlorosalicylic acid occupying the catalytic pocket in close proximity to the catalytically relevant residues Tyr55, His117, and His222. As the 3C3U study reported no apparent induced fit relative to the previously described 20R-hydroxyprogesterone complex 1MRQ, 3C3U provides a suitable template for modelling bisphenol binding in the AKR1C1 active site.

The working hypothesis was that bisphenols would bind within the main AKR1C1 substrate-binding cavity, which normally accommodates progesterone. This model follows the mechanism described by Penning and Drury [62], in which NADP(H) binds before steroid substrate to form the central ternary complex. Because AKR1C1 inhibitor structures have been reported as cofactor-bound enzyme-inhibitor ternary complexes, and because AKR1C1 predominantly operates in the reductive, NADPH-dependent direction *in vivo*, we prioritized E·NADPH·bisphenol models as the primary test case. Nevertheless, it cannot be rule out an alternative mode in which bisphenols bind closer to the NADPH-binding region and potentially interfere with cofactor binding. We therefore first created a baseline E·NADPH·progesterone model using the 3C3U structural template as an approximation of the cofactor-bound active-site geometry. Docking was used to generate candidate substrate- and inhibitor-bound complexes, which were evaluated by short-timescale MD simulations for pose stability.

Detailed computational protocols are described in the Supplementary Methods.

2.11. Enzyme activity assay

The AffiASSAY® Aldo-keto Reductase Activity Assay Kit (colorimetric) (AffiGEN, Vancouver, Canada) was used to assess the change in activity of recombinant AKR1C1 (R&D systems, specifications see 2.9) when exposed to the different bisphenols and AKR1C1 inhibitor, 3-bromo−5-phenylsalicylic acid. The assay was performed twice (n = 2), with two technical replicates in each run, and according to the manufacturer's instructions. The enzymatic activity (nmol/min; mU) was calculated dividing the slope of the sample reaction (OD/min) by the slope of the standard curve (OD/nmol). Mean activity values (mU) across runs were calculated. Relative activity was determined against the AKR1C1 + 0.1% DMSO control and is presented as mean ± SD between runs.

2.12. Statistical analysis

Statistical analysis for lipid accumulation assay (2.2), adipokine release (2.4), metabolite analysis (2.6) and nanoDSF (2.9) was performed in GraphPad Prism Software (version 10, La Jolla, CA, USA). Data are presented as mean ± standard deviation (SD). Differences in lipid accumulation and adipokine release following bisphenol exposure were analyzed using Brown-Forsythe and Welch ANOVA tests. Differences in melting points were analyzed using ANOVA followed by Dunnett's multiple comparisons test. Significant changes in relative metabolite abundances were analyzed by a Welch ANOVA test followed by a Games Howell post hoc test.

3. Results

3.1. Altered lipid accumulation in SGBS cells following bisphenol exposure

To determine the effects of bisphenols on cell viability, SGBS cells were exposed to the concentrations, ranging from 1 nM to 1 mM (Fig. 1A,B) throughout the 12-day adipogenic differentiation period. These two setups were included since the toxicity of the chemicals may differ depending on the adipogenic state of the cells. Cell viability was determined by quantifying DAPI-stained DNA.

Cytotoxicity was overall much higher in cells treated with rosiglitazone during exposure, indicating that cells undergoing rosiglitazone-induced adipogenic differentiation were more susceptible to the cytotoxic effects of these chemicals (Fig. 1B,C). TBBPA and TCBPA showed the highest cytotoxicity (IC_{20} TBBPA = 8.17 μM (5.52 – 11.72), IC_{20} TCBPA = 9.74 μM (4.66 – 18.33). From least to highest toxicity the bisphenols can be arranged as follows: BPS < TCBPS < BPA < TBBPS < TCBPA < TBBPA. Generally, the halogenated derivates of bisphenols A showed higher toxicity. The higher toxicity of TBBPA and TCBPA (IC_{20} ~ 10 μM) needs to be considered when interpreting further experiments with these chemicals at higher concentrations. Although 10 μM TBBPA and TCBPA induced a moderate reduction in cell viability, this concentration was retained to maintain a consistent experimental design and facilitate comparison of molecular responses.

Next, the effect of the different bisphenols on adipogenesis was assessed by exposing SGBS pre-adipocytes to a concentration range of 1 nM to 100 μM to the bisphenols for 12 days during differentiation, similar to the determination of cell viability. The experiment was performed both in the absence (Fig. 1D) and in the presence (Sup. Fig. 1) of rosiglitazone.

Overall, all bisphenols, except BPA, induced a concentration-dependent increase in lipid accumulation during adipogenesis in SGBS cells (Fig. 1D). The increase in differentiated adipocytes is also visible in fluorescence picture documentation (Sup. Fig. 1B). These effects, however, were only visible in the absence of rosiglitazone. When the synthetic PPARγ ligand was present, no significant changes in lipid accumulation for halogenated BPS alternatives were detected (Sup. Fig. 1A).

In the absence of rosiglitazone (Fig. 1D) both halogenated BPA alternatives, TBBPA and TCBPA, led to a significant increase in triglyceride content in cells in the low to mid concentration range, while concentrations higher than 10 μM led to a decrease in lipid accumulation, likely reflecting increased cytotoxicity at higher concentrations, leading to potential impairments in the ability of cells to store lipids.

BPS and its halogenated alternatives all showed a concentration-dependent increase in triglyceride content, most evident in the mid- to high-concentration range. However, even at concentrations as low as 10 nM, BPS and TCBPS led to a significant increase in lipid accumulation. For BPS, TBBPS, and TCBPS, lipid accumulation reached a plateau at the upper end of the tested concentration range (50–100 μM).

Overall, these results demonstrate the ability of all tested compounds to modulate adipogenesis in human adipocytes. The fact that these effects are only detectable in the absence of rosiglitazone could point towards a potential interaction of the bisphenols with PPARγ.

3.2. Halogenated bisphenols activate human PPARγ

To test the agonistic potential of BPS and its halogenated derivates, TBBPS and TCBPS, to bind and activate PPARγ, the stably transfected HG5LN-GAL4-hPPARγ reporter cell line was used (Fig. 2). Data on the agonistic effects for the other three tested compounds, BPA, TBBPA and TCBPA, with the same experimental setup can be found in Riu et al. [30]. All compounds were first tested on the HG5LN parental cell line containing only the reporter gene to analyze potential toxic effects. Some cytotoxicity was observed at 100 μM, but no specific luciferase activity was detected (data not shown).

BPS treatment only resulted in slight PPARγ activation (Fig. 2). In contrast, the halogenated BPS alternatives were able to activate PPARγ, even though being 100–1000-fold less potent than the pharmaceutical reference PPARγ ligand rosiglitazone. TBBPS showed the strongest activation of PPARγ followed by TCBPS.

3.3. Halogenated BPA alternatives alter adipokine release in SGBS adipocytes

Subsequently, the release of the adipokines adiponectin, leptin, and MCP−1 into the cell culture supernatant of mature SGBS adipocytes following bisphenol exposure was examined (Fig. 3). After the 12-day differentiation process, adipocytes were exposed to 10 nM or 10 μM bisphenols for 24 h, 4 days and 8 days with media changes every 48 h. Additionally, a DMSO, a GW9662 (PPARγ antagonist) and a rosiglitazone (PPARγ agonist) control were included (Fig. 3 A).

Adiponectin is a PPARγ-regulated adipokine with anti-inflammatory and insulin-sensitizing properties [66]. As expected, throughout all timepoints the rosiglitazone treatment led to a significant increase in adiponectin secretion (Fig. 3B). After 24 h, TBBPA, BPS and TBBPS induced a significant increase in adiponectin secretion, while BPA led to a decrease (Fig. 3B). The effects of the bisphenols became more pronounced at later time points (days 4 and 8), with strongest effects of BPS and its halogenated derivatives on adiponectin secretion observed on day 8. In contrast, the other bisphenols did not significantly increase adiponectin secretion.

The hormone leptin signals the hypothalamus the current energy status and control hunger, thereby regulating long-term energy homeostasis [7,67]. High leptin level correlate with high energy storage and increases satiety [67]. As expected, mature adipocytes produced leptin at all invesitgated time points. GW9662-treated adipocytes showed a decrease in leptin secretion (Fig. 3 C), consistent with the PPARγ antagonistic activity of GW9662 leading to reduced lipid storage in adipocytes. All tested bisphenols, except BPA, led to a significant decrease in leptin secretion after 24 h. At later timepoints only the halogenated BPA alternatives TBBPA and TCBPA significantly decreased leptin secretion (Fig. 3 C).

MCP−1 is a key chemokine which recruits immune cells such as monocytes from the blood stream into the tissue in response to inflammation and tissue damage [68]. GW9662-treated cells showed a slight increase in MCP−1 secretion while rosiglitazone caused a decrease (Fig. 3D). This is consistent with the anti-inflammatory properties of PPARγ when activated. Short-term bisphenol exposure (24 h) has led to no significant changes except for TBBPS and TCBPS. After 4 days however, TCBPS exposure increased MCP−1 secretion, along with TBBPA and BPS, while BPA showed a slight decrease. After 8 days, MCP−1 secretion was relatively close to the DMSO control in all bisphenol treatments except for BPA, which was significantly elevated.

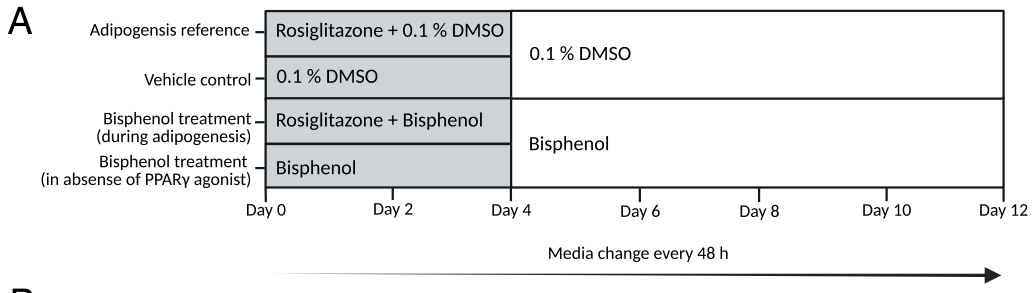

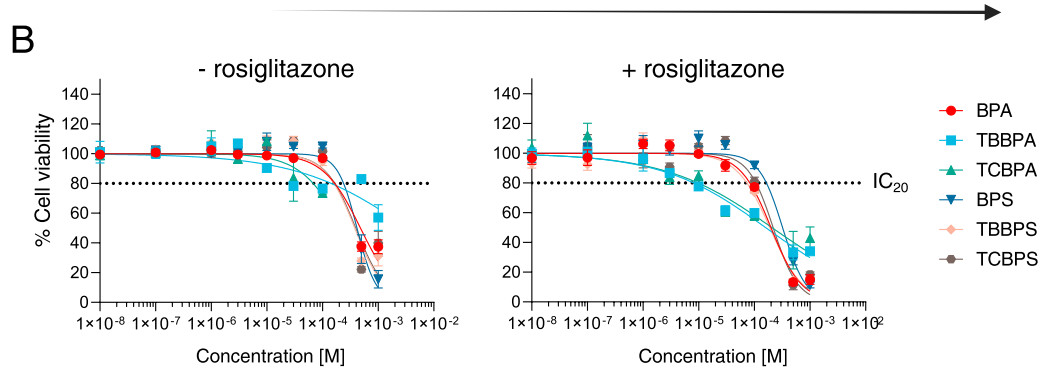

C

IC_{20} [µM] (95 % CI)	BPA	TBBPA	TCBPA	BPS	TBBPS	TCBPS
- rosi	166.2 (122.3–217.2)	143.4 (67.3–266.7)	67.9 (41.6–∞)	239.2 (178.3–306.2)	160.7 (107.3–229.0)	165.9 (98.9–256.2)
+ rosi	83.0 (68.1–100.7)	8.17 (5.52–11.72)	9.74 (4.66–18.33)	165.0 (127.6–210.0)	73.5 (58.7–91.4)	106.8 (81.9–139.7)

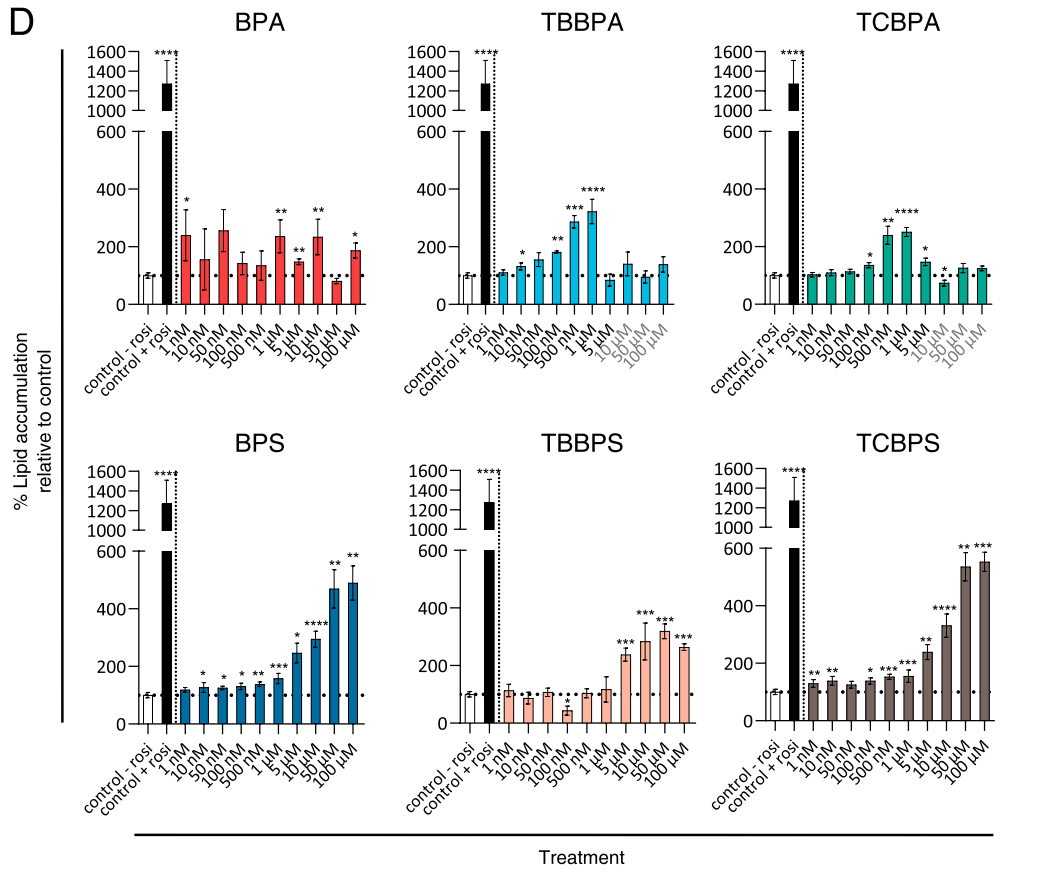

(caption on next page)

Fig. 1. Effects of bisphenols and their halogenated alternatives on cell viability and lipid accumulation in SGBS adipocytes during adipogenesis. (A) Experimental setup. SGBS cells were differentiated over the course of 12 days while being continuously exposed to bisphenols in concentrations ranging from 1 nM to 1 mM. Controls were treated with 0.01% DMSO. Medium was changed every 48 h. (B) Dose-response-curve of cell viability, determined using DAPI-staining on day 12. DAPI fluorescence relative to the vehicle control is shown in % cell viability for cells treated with and without rosiglitazone. (C) Bisphenol concentrations that induce 20% cell viability reduction (IC_{20}), calculated from the concentration-response curves. Depicted as mean (95% CI). (D) Quantification of lipid accumulation on day 12 of differentiation using Nile Red staining normalized to DNA content. Bar charts depict mean ± SD. Statistically significant differences in lipid content against DMSO control were calculated using Brown-Forsythe and Welch ANOVA tests and are indicated by asterisks (* $p \leq 0.05$, ** $p \leq 0.01$, *** $p \leq 0.001$, **** $p \leq 0.0001$). n = 4. Rosi = rosiglitazone. TBBPA, TCBPA > 10 μM are in gray because of cytotoxicity.

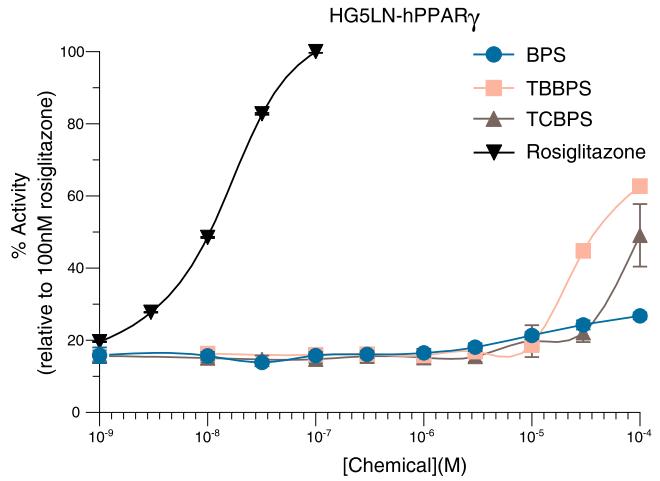

Fig. 2. PPARγ activation assessed by luciferase activity assay. Dose-response curves of BPS and halogenated analogues (TBBPS and TCBPS), as well as PPARγ agonist rosiglitazone in HG5LN-hPPARγ cells. Results are displayed in percentage of luciferase activity measured per well relative to 100 nM rosiglitazone activity. Mean values ± SD are depicted, n = 4.

3.4. Halogenated bisphenol A alternatives increase lipid and energy metabolism

To investigate molecular responses associated with bisphenol exposure in mature adipocytes, a global untargeted proteome analysis was performed (Fig. 4). SGBS adipocytes were differentiated until day 12 and the mature adipocytes were then exposed for 24 h, 4 and 8 days to 10 nM or 10 μM of each bisphenol (experimental setup identical to Fig. 3 A).

In the principal component analysis (PCA, Fig. 4A) a distinct clustering of the treatments becomes more apparent with longer exposure periods. For example, after 24 h the PCA showed no distinct clusters while after 4 days the high concentrations of TBBPA and TCBPA cluster together. Also, cells treated with 10 μM of TBBPS or TCBPS clustered together with the rosiglitazone-treated cells after 4 and 8 days. The datapoints closest to this cluster were the cells treated with 10 μM BPS.

To gain a deeper look into the specific effects of the bisphenols, the significantly up and down regulated proteins were analyzed using KEGG and REACTOME database to identify significantly altered (adjusted p-value ≤ 0.05) pathways (Fig. 4B,C). Both databases revealed that the initial response after 24 h appears distinctly different from the longer incubation periods. Based on the KEGG analysis, pathways connected to protein turnover and cellular maintenance were upregulated for most bisphenol treatments after 24 h. These pathways, namely proteasome and ribosome pathway, were mostly not affected after longer bisphenol exposure, indicating that the treatments initially had an effect on the protein synthesis which later subsided. Instead, signal transduction, cell structure and lipid and energy metabolism became more prominently altered across treatments at later timepoints. REACTOME pathway analysis revealed early increase of proteins associated with pathways such as stress responses and energy metabolism, while prolonged exposure led to increasingly treatment-specific alterations in pathways.

As the PCA clustering has already indicated, the similarities between rosiglitazone-treated cells and cells exposed to BPS and its halogenated alternatives became increasingly apparent at the pathway level. Comparable patterns of pathway up- and downregulation were observed for pathways associated with signal transduction, energy and carbohydrate metabolism, lipid metabolism and cell structure across both databases. Central to this conclusion is the KEGG PPAR signaling pathway, which was significantly upregulated following rosiglitazone treatment as well as BPS, TBBPS and TCBPS exposure. Interestingly, TBBPA and TCBPA did not lead to a significant upregulation of PPAR signaling pathway, apart from 10 μM TCBPA treatment after 4 days.

Interestingly, the halogenated bisphenol S alternatives had an upregulating effect regarding the insulin signaling pathway, while rosiglitazone led to a downregulation of this pathway. The overall similarity with rosiglitazone-treated cells was also visible in the changes in energy metabolism through key pathways such as tricarboxylic acid (TCA) cycle, oxidative phosphorylation, the metabolism of amino acids and the upregulation of pathways connected to lipid metabolism, like fatty acid metabolism or function of peroxisomes. These similarities were also noticeable as a trend at the lower concentrations of TBBPA and TCBPA, although most of these changes did not reach statistical significance. The cytotoxic effect of high concentrations of the BPA alternatives was also visible on pathway level through the down regulation of key energy and lipid metabolic pathways. Interestingly, KEGG pathways connected to lipid metabolism were upregulated after 4 days of exposure of TBBPA and TCBPA and downregulated after 8 days. Also, cell structure-associated pathways from both databanks were downregulated for the high concentrations of all tested bisphenols except BPA (Fig. 4B,C). A similar effect was visible in the rosiglitazone-treated cells throughout all timepoints. Overall, the least effects were visible following BPA treatment, except for KEGG steroid hormone biosynthesis, REACTOME glucocorticoid biosynthesis pathways, which were significantly upregulated after 4 days. GW9662 treatment resulted in slight, mostly non-significant changes. An extended analysis of the proteomics results can be found in the supplements (Sup. Fig. 3).

Overall, these findings demonstrate that halogenated bisphenols modulate key metabolic and signaling networks in adipocytes. While halogenated BPS alternatives showed similarities to the rosiglitazone treated cells, TBBPA and TCBPA induced proteomic alterations that only partially overlapped with the rosiglitazone-like PPARγ activation signature, suggesting the involvement of additional, PPARγ-independent mechanisms.

3.5. Halogenated bisphenols lead to changes in TCA cycle

In light of the found modulation of key energy-related metabolic pathways, we investigated the effect of the bisphenols on metabolites of the central carbon cycle. For this, mature SGBS adipocytes were exposed to 10 nM and 10 μM of bisphenols before being harvested after 24 h and 8 days. Metabolites were extracted and analyzed using LC-MS/MS. Rosiglitazone, GW9662, and a DMSO control served as reference conditions (Fig. 5).

Consistent with the proteome data, metabolic alteration became more pronounced with prolonged bisphenol incubation (Fig. 5). Rosiglitazone-treated cells showed a general increase in glycolysis metabolites and a decrease in TCA cycle metabolites and amino acids. GW9662-treated cells generally showed very limited effects.

For TBBPA and TCBPA exposure, differences are visible between

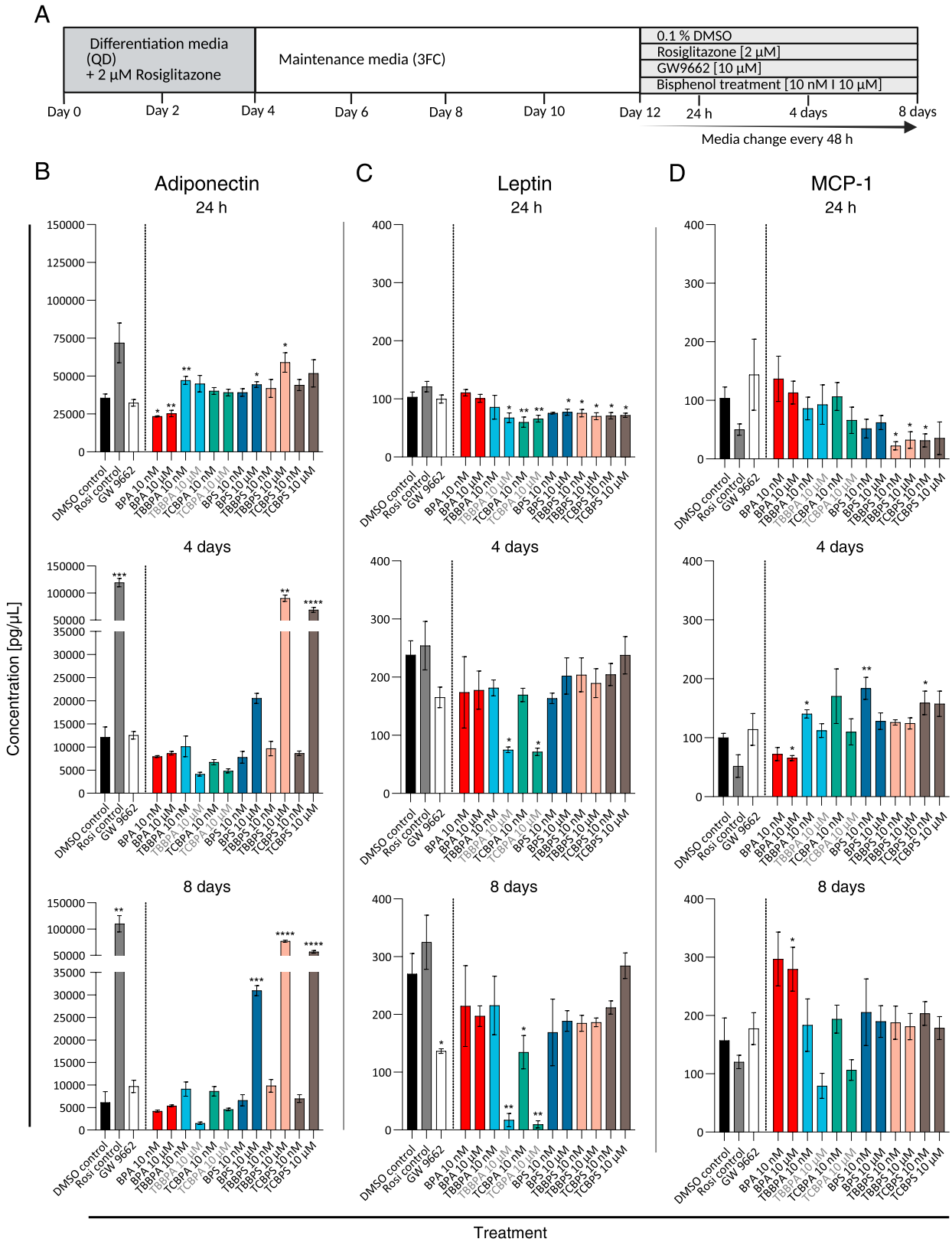

Fig. 3. Adipokine secretion of mature SGBS adipocytes after bisphenol exposure. (A) Experimental setup: Mature SGBS cells were exposed for 24 h, 4 days and 8 days with medium changes every 48 h. The release of the adipokines (B) adiponectin, (C) leptin, and (D) MCP−1 were quantified in the supernatant at each timepoint using ELISA. Bar charts depict mean ± SD, n = 4. Statistically significant differences against DMSO control of each respective timepoint were calculated using Brown-Forsythe and Welch ANOVA tests and are indicated by asterisks (* $p \leq 0.05$, ** $p \leq 0.01$, *** $p \leq 0.001$, **** $p \leq 0.0001$). Rosi = rosiglitazone. 10 µM TBBPA and TCBPA are in grey due to elevated cytotoxicity.

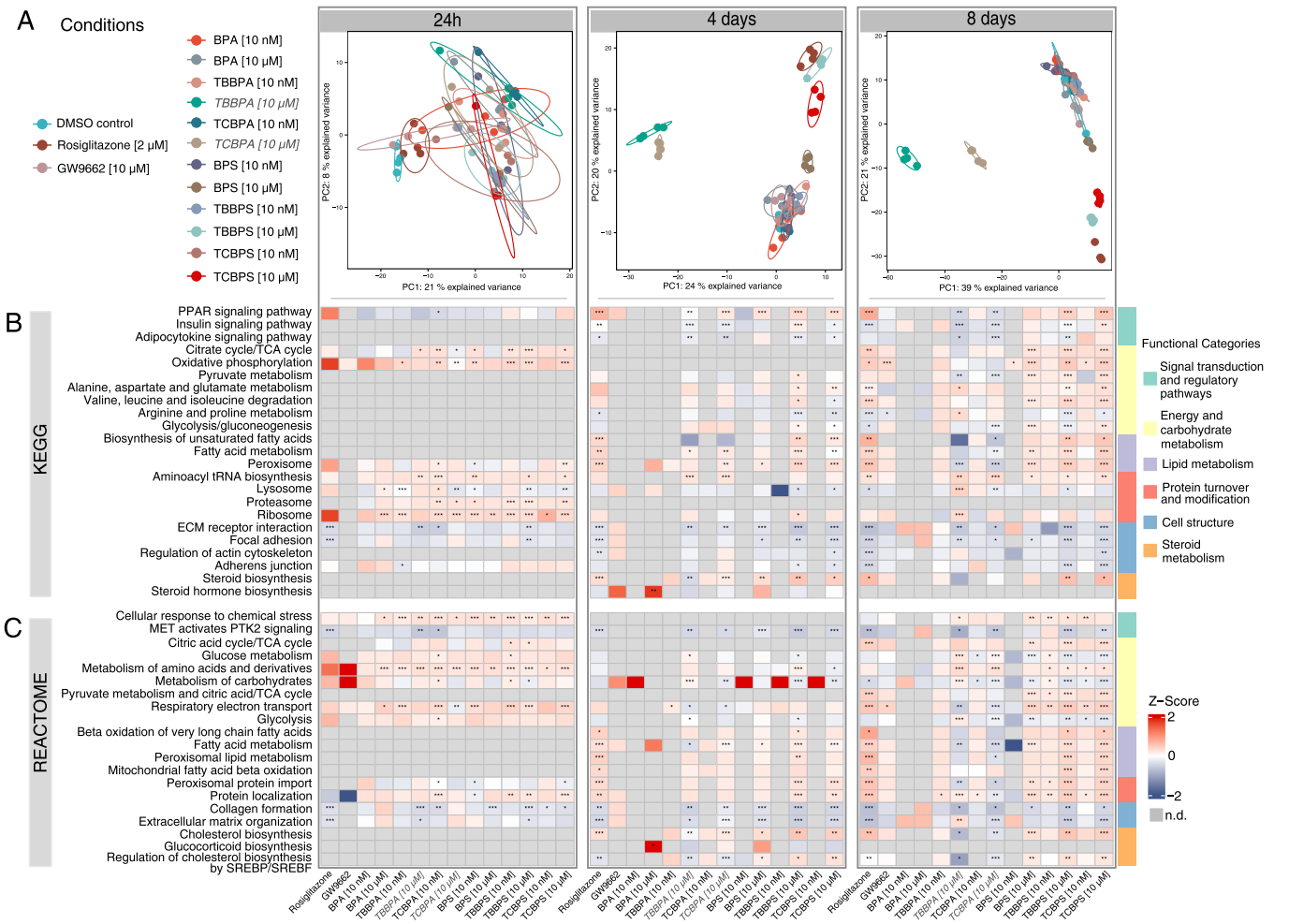

Fig. 4. Proteome analysis of halogenated bisphenols in mature SGBS adipocytes. (A) PCA of all analyzed data separated by the three different timepoints. (B) Heatmap of selected significantly altered (p value ≤ 0.05, Student's *t*-test followed by Benjamini-Hochberg correction and are indicated by asterisks (* $p \leq 0.05$, ** $p \leq 0.01$, *** $p \leq 0.001$, **** $p \leq 0.0001$)) pathways in treated SGBS adipocytes analyzed with database KEGG and (C) REACTOME. Functional categories of pathways are indicated. Z-score indicates the direction of pathway regulation (z-score > 0 = pathway is upregulated, z-score < 0 = pathway is down-regulated, NA is indicated in grey, n = 4). 10 µM TBBPA and TCBPA are in grey due to cytotoxicity.

used concentrations and incubation time points. Acute exposure to low concentrations generally led to an increase in most metabolites, including glycolysis, pentose phosphate pathway (PPP) and the TCA cycle. In contrast, both time points after treatment with high concentrations of TBBPA and TCBPA resulted in a significant reduction of the aforementioned metabolites. This likely reflects their increased cytotoxicity.

Both concentrations of BPA caused similar alterations in metabolite levels to the high concentrations of its halogenated derivates. BPA specifically decrease Frc6B, Glc6P and Frc1,6BP, which all function in the upper steps of the glycolysis, while the rest of this metabolic pathway remained mostly unchanged (Fig. 5B).

Both concentrations of BPS and its halogenated alternatives led to an overall increase in metabolites connected to glycolysis, the PPP and nearly all TCA cycle-related metabolites, particularly AcCoA and MaCoA, with more pronounced effects observed after 8 days (Fig. 5A,B). Overall, BPA and its halogenated derivates overall show opposing effects on the analyzed metabolites compared to BPS and its alternatives.

In summary, halogenated bisphenols induced distinct yet coherent alterations in central carbon metabolism in human adipocytes, revealing clear compound class-specific effects. BPS and its halogenated analogues exhibited highly similar metabolic profiles, characterized by a broad accumulation of glycolysis-intermediates as well as PPP and TCA cycle-related metabolites, indicating a pronounced perturbation of central carbon metabolites. In contrast, BPA and its halogenated derivatives displayed a more heterogeneous but internally consistent response pattern, including alterations in upper glycolysis and amino acid metabolism.

3.6. *Identification of putative intracellular target proteins of BPA and halogenated alternatives*

The analysis of the proteome of the cells treated with some of the halogenated bisphenols pinpoints to a modulation of pathways beyond PPARγ activation. Thus, TPP was used to identify unknown potential cellular target proteins (Fig. 6). TPP is a method used to identify molecular protein targets, usually of small molecules like drugs (or chemicals), metabolites or other proteins within the proteome of cells or lysates [46]. It utilizes the fact that protein thermal stability can be influenced by interaction with other molecules.

In our setup, we used TPP to identify molecular targets in lysates of mature SGBS cells (Fig. 6A). Cell lysates were incubated with the bisphenols, heated over a temperature gradient and the non-denatured protein fraction was then quantified by LC-MS/MS. The melting point (T_m) is defined as the temperature, at which 50% of the protein compared to the lowest incubation temperature (37.1 °C) is not detectable, indicating protein denaturation. Binding between the proteins in the lysates and the bisphenols is indicated through a difference

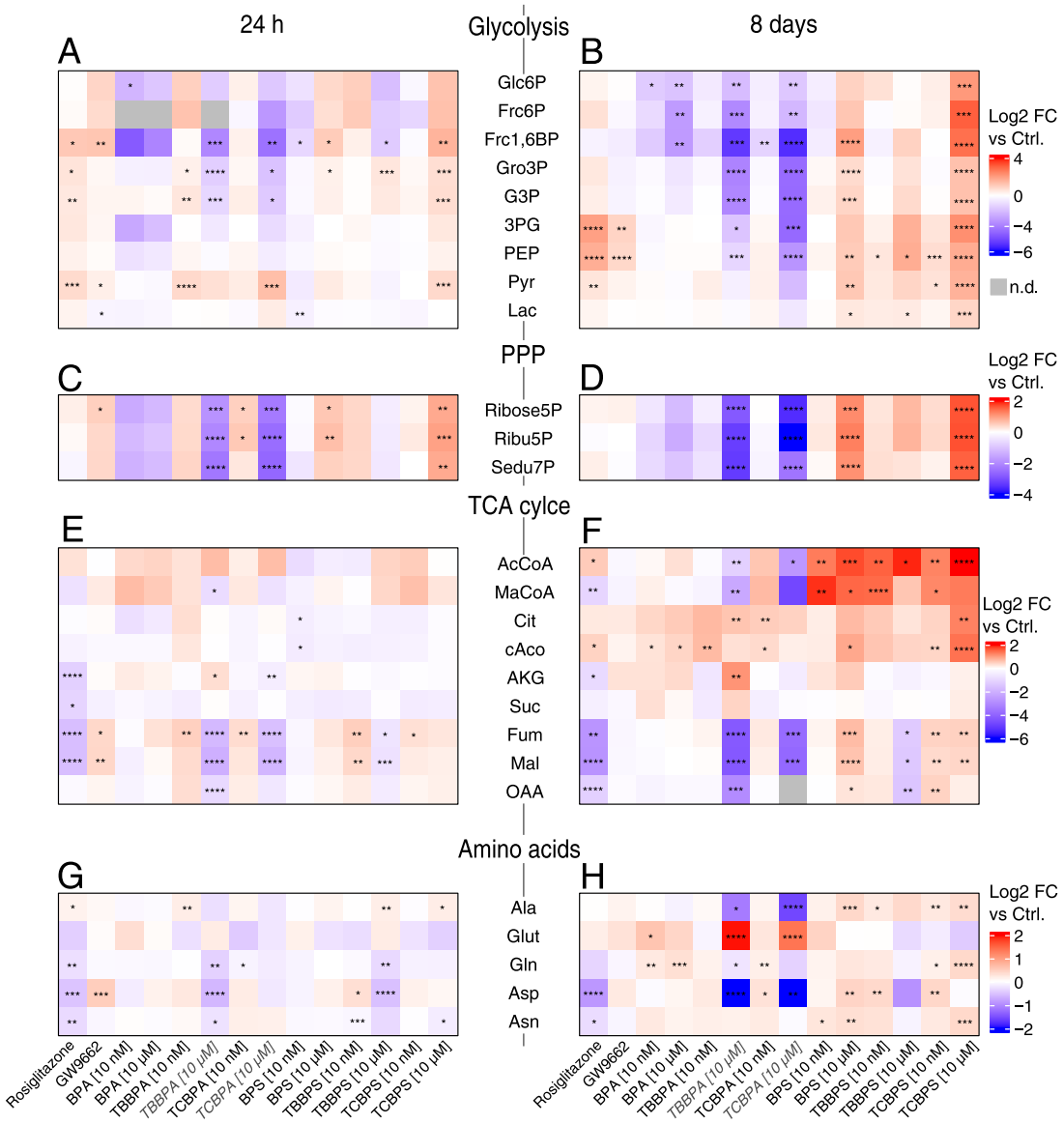

Fig. 5. Effects of bisphenols on central carbon metabolism. Major SGBS adipocytes were exposure to bisphenols for 24 h and 8 days, respectively. Metabolites are subdivided into (A,B) glycolysis, (C,D) PPP, (E,F) TCA cycle and (G,H) amino acids. Data is displayed as Log2 FC, relative to control conditions. Welch ANOVA followed by Games-Howell post-hoc test was performed to calculate statistical significances, which are indicated as following: * = $p \leq 0.05$, ** = $p \leq 0.01$, *** = $p \leq 0.001$, **** $p \leq 0.0001$. n = 4. Abbreviations: 3PG - 3-phosphoglycerate, Frc1,6BP - fructose 1,6-bisphosphate, Frc6P - fructose 6-phosphate, G3P - glyceraldehyde 3-phosphate, Glc6P - glucose 6-phosphate, Gro3P - glycerol 3-phosphate, Lac - lactate, PEP – phosphoenolpyruvate, Pyr – pyruvate, Ribose5P - ribose 5-phosphate, Ribu5P - ribulose 5-phosphate, Sedu7P - sedoheptulose 7-phosphate, AcCoA – AcetylCoA, AKG – α-ketglutarate, cAco – cis-aconitate, Cit – citrate, Fum - fumarate, Mal – malate, MaCoA - malonyl-CoA, OAA - oxaloacetate, Suc – succinate, Ala - alanine, Asp - aspartate, Asn - asparagine, Glut - glutamate, Gln – glutamine.

in melting point (ΔT_m) compared to the vehicle-treated control (0.01% DMSO).

In total, 3082 proteins were identified by LC-MS/MS between all setups (Fig. 6B). All reliably identified proteins (identified in 3 out of 4 replicates per condition, 1st) per setup are indicated in a bar chart (Fig. 6B). Candidate proteins were selected based on melting curve quality, reproducibility and significant compound-induced thermal shifts (see Methods 2.8).

Most candidate proteins were identified in the TBBPS treatment (27), followed by BPS (21), TCBPS (16), TCBPA (13) TBBPA (5) and lastly BPA (2). There was considerable overlap of candidate proteins between bisphenol treatments (Fig. 6C). This is probably due to the structural similarity between the bisphenols. The overlap was particularly visible in the BPS and its analogues. Of the 27 candidate proteins identified in TBBPS-treated samples, four were shared with TCBPS (AKR1C2, PRCP, PSMD14, CRYAB) and 3 with BPS (SCRN2, CAPN2, STON1). Volcano plots (Sup. Fig. 4) and a full list of all candidates, including full names can be found in supplements (Sup. Table 1).

The common denominator between these three bisphenols was AKR1C1. AKR1C1 showed the largest shift in thermal stability following bisphenol treatment ($\Delta T_{m,BPS} = +6.3$ °C (±0.7 °C); $\Delta T_{m,TBBPS} = +2.0$ °C (±0.7 °C); $\Delta T_{m,TCBPS} = +3.9$ °C (±1.1 °C), Fig. 6E). However, it was not the only enzyme within this subfamily to stand out as a target protein of BPS and its halogenated alternatives. Both BPS ($\Delta T_m = +1.1$ °C (±0.5 °C)) and TCBPS ($\Delta T_m = +1.2$ °C (±0.5 °C)) lead to a stabilization of AKR1C2, and TBBPS ($\Delta T_m = +0.4$ °C (±0.1 °C)) and TCBPS ($\Delta T_m = +0.4$ °C (±0.2 °C)) led to a stabilization of AKR1C3. The clustering of the proteins within the aldo-keto reductase superfamily is demonstrated in the string network (Fig. 6D). These results suggest the interactions between structurally similar bisphenols and multiple enzymes within the

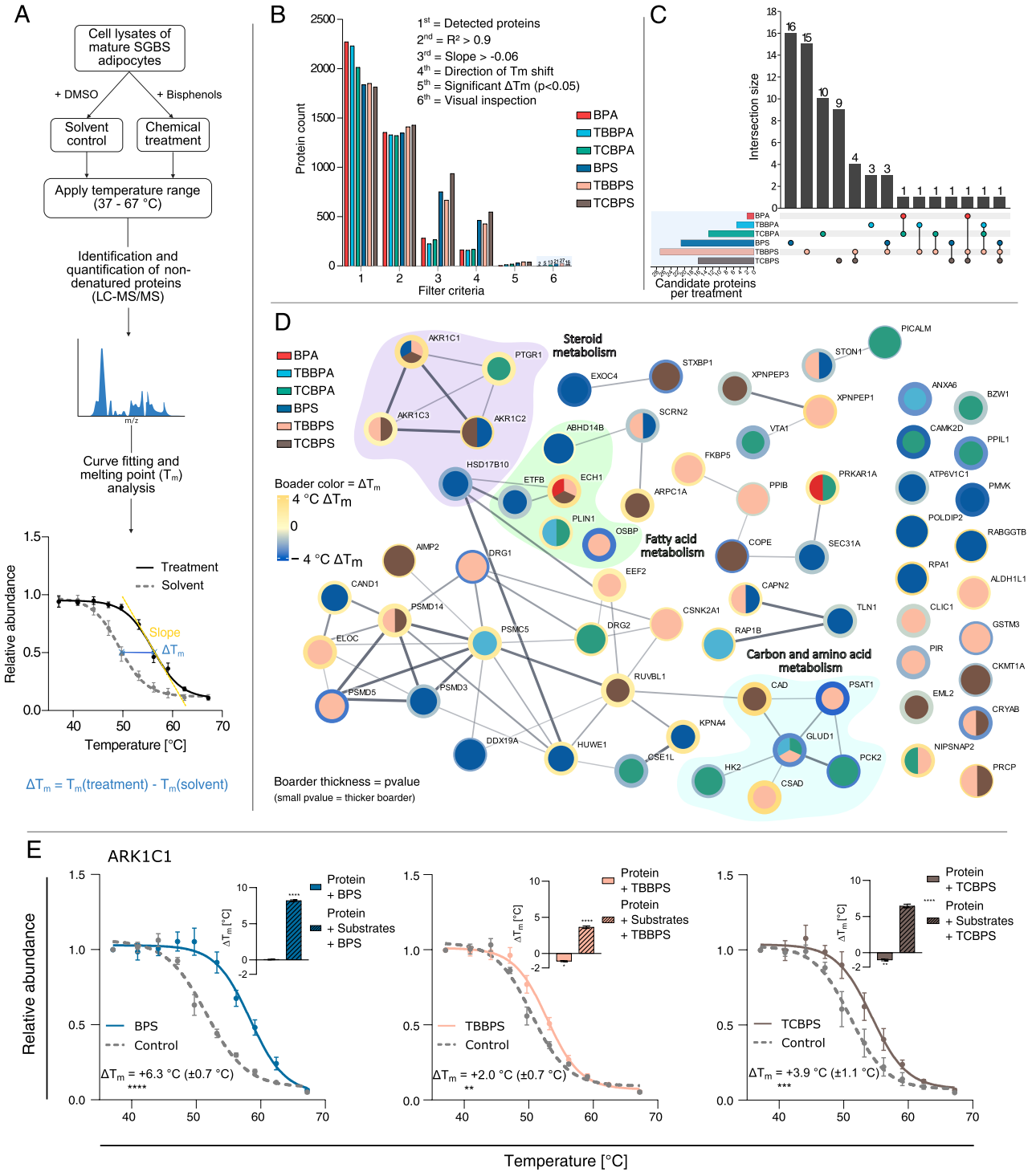

Fig. 6. Identification of putative molecular target proteins of halogenated bisphenols in SGBS cell lysates using TPP. (A) Methodological overview. Mature SGBS adipocytes were harvested and lysed. Lysates were incubated with 10 μM bisphenols or DMSO, respectively. Treated lysates were heated over a temperature gradient from 37.1 to 67.2 °C. The fraction of non-denatured proteins was identified using LC-MS/MS. Melting curves for each protein were fitted over remaining protein abundance per temperature point. Bisphenol-treated samples were compared to vehicle control to identify shifts in melting point. n = 4. (B) Total number of identified proteins and consecutive filtering criteria applied to identify candidate proteins. (C) Overlap of TPP-identified candidate proteins between bisphenol treatments, showing unique and shared candidates per compound. Color of proteins indicates specific bisphenol that induced thermal shift, boarder color indicates direction of shift (yellow = stabilization, blue = destabilization) and boarder thickness indicates p.value (thicker = smaller p value). Nodes between proteins show connectivity, based on cellular compartments, protein family and expression tissue. If multiple bisphenols induced shift, mean p.value and ΔT_m were calculated between all treatments. Functional clusters are indicated by colored backgrounds. (E) Melting curves of candidate protein AKR1C1. Significance of thermal shift between vehicle control and bisphenol treatment was calculated using Student's *t*-test. Bar chart of nanoDSF validation of respective protein is displayed for each melting curve. ΔT_m of protein + bisphenol setup was calculated relative to the T_m of the protein-only reference, ΔT_m of protein + substrate + bisphenol setup is relative to T_m of protein + substrate reference. Plain bar indicates setup without the natural substrate, striped bar indicates setup with the natural substrate.

same subfamily.

To confirm TPP results, binding of bisphenols to selected candidate proteins (AKR1C1, GLUD1, PSAT1, PMVK) were analyzed by nanoDSF (Sup. Fig. 5). This type of thermal shift assay uses the intrinsic fluorescence of tryptophan within the protein. Temperature-dependent changes of fluorescence during unfolding were quantified and used as a readout to determine bisphenol-induced shifts in protein thermal stability. Due to the structural similarity between the tested bisphenols (Sup. Fig. 1B) and the overlap in candidate target proteins between treatments, all bisphenols were analyzed with each of the candidate proteins (Sup. Fig. 5). To enable direct comparison between the TPP and nanoDSF experiments, the corresponding nanoDSF results were additionally presented as a bar chart alongside the AKR1C1 TPP melting curves (Fig. 6E).

BPS and its halogenated derivates induced a stabilizing effect on AKR1C1 in the TPP experiment, with the strongest T_m shift observed in this experiment (Fig. 6E). A similar shift was detected during nanoDSF experiments when AKR1C1 was incubated together with its natural substrate, progesterone and NADPH (Fig. 6E). The infliction point shifted significantly with + 1.4 °C. Sole treatment with bisphenol did not induce a significant thermal shift in AKR1C1 (compared to protein reference, Fig. 6E, Sup. Fig. 5A,B). However, upon incubation with the natural substrates, the bisphenols all induced varying levels of stabilization (compared to protein + substrates reference), with TCBPA leading to the strongest shift of + 11.6 °C. In experiments only including cofactor NADPH without progesterone, the bisphenols showed a similar thermal stabilization as with both NADPH and progesterone present (Sup. Fig. 6), demonstrating the conformational change induced by cofactor binding on AKR1C1 [69].

Another target protein identified across multiple treatments was GLUD1, a mitochondrial enzyme linking amino acid and carbon metabolism [70], which clustered together with proteins involved in these functional categories in the STRING network analysis (Fig. 6D). Consistent with the TPP results, GLUD1 showed reproducible destabilization in nanoDSF upon treatment with several bisphenols as well as its natural substrates (Sup. Fig. 5D-F), supporting its potential relevance as a target protein.

Similar effects were observed for PMVK, although substrates alone led to a stabilization of the protein while both with and without substrates TBBPA and TCBPA led to a destabilization of the protein (Sup. Fig. 5G-I). Additionally, nanoDSF revealed marked changes in melting curve shape upon substrate or bisphenol treatment (Sup. Fig. 5G–I). Without its natural substrate PMVK has a broader melting curve while the addition of the substrate as well as the two bisphenols led to narrower melting curves with less pronounced shoulders.

PSAT1 behaved differently compared to the other proteins: substrate binding induced a strong stabilizing shift and substantially altered the melting behavior, while bisphenol treatments caused less conventional fluorescence profiles and pronounced curve shape changes Sup. Fig. 5J-L). Overall, several candidate proteins identified in TPP could be confirmed by nanoDSF, whereas others showed more complex or less consistent thermal behavior.

The identification of novel molecular interaction targets of halogenated bisphenols revealed both shared and compound-specific protein interactions. In particular, the AKR1C1-bisphenol interaction detected by TPP was consistently reproduced across experimental setups, with nanoDSF confirming a coherent directionality of thermal stability shifts. Due to its clear biological relevance and robust, reproducible thermal responses, AKR1C1 emerged as a prominent molecular target. However, it is important to note that the induction of a thermal shift alone does not indicate whether the identified interaction is of activating or inhibitory nature. To address this, a functional characterization including enzyme activity assay was performed to determine the functional consequences of the observed interactions.

3.7. AKR1C1 inhibition shows similarities to halogenated BPS alternatives on proteome level

To unravel the functional relevance of the novel identified bisphenol-interacting proteins, we chemically inhibited AKR1C1 in SGBS adipocytes using 3-bromo−5-phenylsalicylic acid (Fig. 7A) and analyzed the global proteome, as well as the metabolites of the central carbon metabolism. This experimental setup is further supported by the observation that 3-bromo−5-phenylsalicylic acid induced a thermal shift in AKR1C1 during nanoDSF comparable to those observed for the tested bisphenols (Sup. Fig. 7). For this, cells were treated as described previously for the bisphenol exposure experiments (proteome, 2.5; metabolome, 2.6).

Similar to the bisphenol-treated cells (Fig. 4), longer incubation periods generally resulted in more pronounced changes in pathway regulation (Fig. 7B,C). The PPAR signaling pathway was significantly upregulated following exposure to the AKR1C1 inhibitor at the highest tested concentration after four days of treatment and onwards (Fig. 7B). This initially suggested potential PPARγ activation, specifically given the structural similarities between the inhibitor and the brominated BPA alternative TBBPA (Fig. 7B, Sup. Fig. 1B). However, reporter gene assays revealed no activation of PPARγ by the AKR1C1 inhibitor (data not shown). Despite the absence of direct PPARγ activation, treatment with this AKR1C1 inhibitor led to an upregulation of pathways connected to energy and lipid metabolism, resembling the response observed in rosiglitazone-treated cells (Fig. 4, Fig. 7), as well as in cells exposed to halogenated bisphenols S alternatives, which did show PPARγ agonistic activity (Fig. 2). Furthermore, the inhibitor induced a downregulation of pathways associated with cell structure, again demonstrating similarity to rosiglitazone and halogenated BPS treatment. Even though AKR1C1 is primarily involved in sex steroid metabolism and xenobiotic detoxification, no pathways directly linked to (sex) steroid hormone metabolism or xenobiotic detoxification were significantly altered following inhibitor treatment (Fig. 7B,C). For a better comparison between the bisphenol and the inhibitor treatment a heatmap containing all treatments can be found in the supplements (Sup. Fig. 3).

Analysis of central carbon metabolites following AKR1C1 inhibition (Sup. Fig. 8) revealed the most pronounced effects after 8 days of treatment. Prolonged inhibition led to an increase in TCA cycle-associated metabolites, particularly MaCoA and AcCoA. While amino acid levels remained largely unchanged, AKR1C1 inhibition strongly affected glycolysis and the PPP, resulting in a marked accumulation of associated metabolites. Notably, this metabolic profile closely resembled that observed in cells exposed to halogenated BPS analogues, particularly TCBPS after 8 days (Fig. 5), highlighting striking similarities across PPP, glycolysis, and TCA cycle perturbations.

As binding data alone does not reflect if enzyme activity is also altered, we next analyzed AKR1C1 activity after incubation with the different bisphenols compared to its inhibitor. The results demonstrated that all tested bisphenols exerted an inhibitory effect on AKR1C1 (Fig. 7E). However, BPA (% activity: 80.67% ± 2.41) and TBBPA (68.86% ± 12.03) did not reduce enzyme activity below the level observed for the reference inhibitor 3-bromo−5-phenylsalicylic acid (65.47% ± 2.23). In contrast, all other bisphenols reduced enzyme activity to below 40% of the native enzyme, with TCBPS showing the strongest inhibition (16.23% ± 5.2). Except for TCBPA, the inhibitory effects observed for BPS and its halogenated analogues are consistent with the interactions identified in the TPP experimental setup, where these compounds induced the most pronounced thermal shifts (Fig. 6E).

In summary, functional inhibition of AKR1C1 resulted in proteomic and metabolic alterations that partially overlapped with those observed following exposure to BPS and its halogenated analogues. Although no direct PPARγ activation was observed in our experiments, AKR1C1 inhibition induced alterations in pathways associated with energy and lipid metabolism as well as changes in structural processes, partially resembling responses observed in rosiglitazone- and BPS-, TBBPS-, and

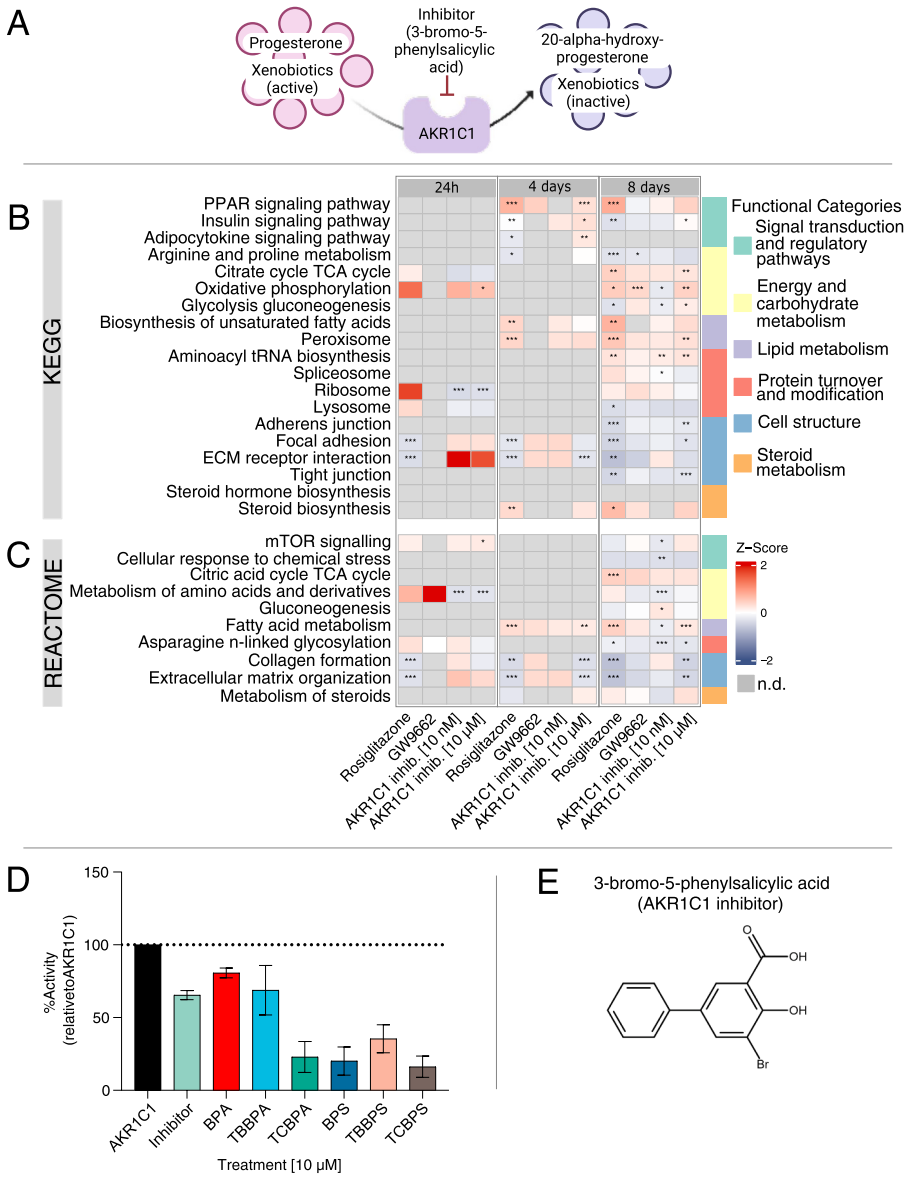

Fig. 7. Effect on pathways after inhibition of AKR1C1 SGBS adipocytes. (A) Metabolic function of target enzyme AKR1C1. (B) Heatmap of selected significantly altered (p.adjust < 0.05) pathways in treated SGBS adipocytes using KEGG and (C) REACTOME database. Functional categories of pathways are indicated. Z-score indicates the direction of pathway regulation (z-score > 0 = pathway is upregulated, z-score < 0 = pathway is down-regulated, NA is indicated in grey, n = 4). Significantly regulated pathways are identified using Student's *t*-test followed by Benjamini-Hochberg correction and are indicated by asterisks (* $p \leq 0.05$, ** $p \leq 0.01$, *** $p \leq 0.001$, **** $p \leq 0.0001$). Functional categories of pathways are indicated. (D) Enzyme activity assay results. Effect of bisphenols and AKR1C1 inhibitor on enzyme activity of recombinant AKR1C1 protein was tested. Nmol/min (mU) was calculated from slope of samples (OD/min), divided by slope of standard curve (OD/nmol). Values are displayed in percent activity relative to AKR1C1 + 0.1% DMSO, as means with ± SD. n = 2. (E) Structure of inhibitor 3-bromo−5-phenylsalicylic acid.

TCBPS-treated cells. At the metabolite level, prolonged inhibition led to a pronounced increase in glycolytic, PPP, and TCA cycle- associated metabolites, showing similarities to the metabolic alterations observed specifically in TCBPS-treated cells. Enzymatic activity assays further demonstrated that exposure to BPS and its halogenated alternatives strongly inhibited AKR1C1, with effects exceeding those of the selective inhibitor 3-bromo−5-phenylsalicylic acid. Collectively, these findings identify AKR1C1 as a functionally relevant target and indicate that especially halogenated BPS alternatives exert their effects, at least in part, through inhibitory interaction with this enzyme.

3.8. In silico modelling of bisphenol binding supports a cofactor-dependent binding mode in AKR1C1

To generate initial ternary models of bisphenol binding, we performed molecular docking of BPA, BPS, and TCBPA into the catalytic pocket of human AKR1C1 using PDB entry 3C3U, a crystal structure containing bound NADP + and the inhibitor 3,5-dichlorosalicylic acid. In this structure, the inhibitor occupies the steroid/inhibitor pocket adjacent to NADP + , in close proximity to the active-site residue cluster Tyr55, His117, and His222. The top-ranked bisphenol poses clustered in the same general region, consistent with the reference geometry. However, because this system represents a ternary ligand–cofactor binding problem, identifying energetically optimized binding poses from docking alone is not straightforward. Established docking workflows do not

support simultaneous placement of multiple ligands within the same binding site, and the final arrangement is also expected to depend on local induced-fit adjustment relative to the cofactor and neighboring side chains. We therefore retained two to four top-ranked poses per ligand for short replicated MD simulations, which were used to refine the ligand-cofactor geometry and identify the most stable modelled ternary binding mode.

MD simulations were then used to examine whether the docked bisphenol poses behaved differently in the pocket. Since ligand root-mean-square deviation (RMSD) alone does not indicate whether the ligand retains a similar geometry in relation to the cofactor, we monitored protein/bisphenol/cofactor RMSD alongside representative catalytic/cofactor-proximal distances. Across all replicas, bisphenols remained within the steroid/inhibitor pocket. There was no persistent drift into alternative pockets, repeated switching between binding modes or ligand ejection. Within this stable ensemble, trajectories with the closest ligand–cofactor association converged towards a shared pose family within the same general active-site region occupied by progesterone (see Fig. 8). In this refined arrangement, minor repositioning of the nicotinamide group enabled closer association between the ligand and cofactor, as reflected by the monitored distance metrics (see Sup. Fig. 9).

Next, we asked whether this structural refinement was reflected in the end-point energy estimates, and whether these estimates reproduced the differences in inhibitory activity observed experimentally among bisphenol variants. Molecular mechanics-based generalized Born and Poisson-Boltzmann surface area calculations (MM-GBSA and MM-PBSA) were therefore applied to all replica trajectories. Within each ligand series, the most favorable scores were associated with deeper, cofactor-proximal poses that defined the shared bisphenol pose family described above. However, the GB- and PB-based estimates differed substantially and the inter-replica standard deviations of 2–4 kcal/mol were comparable to or larger than the energetic differences between the bisphenol complexes, including the average separation between BPA and BPS. The end-point calculations were therefore not interpreted as quantitative relative binding affinities.

Our *in silico* results support a common cofactor-dependent ternary binding mode for the bisphenol series, but they do not explain the experimentally observed differences in inhibitory potency between individual analogues, such as BPA and BPS. MD simulations identified a family of shared low-energy poses in which the local rearrangement of NADPH and nearby side chains produced a deeper binding mode for bisphenols in the steroid/inhibitor pocket than was captured by the initial docking poses. These ternary complexes therefore provide a basis for future alchemical relative free energy calculations, in which one bisphenol analogue is gradually transformed into another in both the bound and unbound states. This would allow for a more robust estimation of free energy differences between bisphenols than was possible with end-point calculations.

4. Discussion

BPA is an extremely prevalent environmental pollutant, detectable in most individuals in the general population [48] and is linked to multiple adverse health effects [71]. Specifically, it is associated with disruption of endocrine function across various targets, such as the reproductive system, and adipose tissue [13]. Multiple studies have also described adipogenic properties of BPA. Urinary BPA levels correlate with waist circumference, obesity [14,49] and certain comorbidities like type 2 diabetes [18]. These concerns have led to the development of BPA alternatives. Studies investigating the impact of emerging BPA alternatives point to analogues having similar or potentially stronger effects regarding metabolic perturbation [24,29,31,72].

In the present study, the SGBS cell culture system was used as they closely resembles primary human adipocytes, when differentiated [54]. Even though they represent a well-established model for the investigation of adipocyte differentiation, metabolism and biology, multiple limitations should be considered. As with any cell culture system, they remain an *in vitro* model that cannot fully reproduce the cellular complexity and endocrine regulation of human adipose tissue. In particular, interactions with immune cells, endothelial cells, fibroblasts, and systemic hormonal regulation are absent. Therefore, the identified molecular mechanisms should be interpreted as mechanistic hypotheses that require validation in primary human adipocytes, more complex multicellular adipose tissue models, and ultimately *in vivo* studies to determine their physiological relevance and contribution to human health risks.

We focused on halogenated bisphenols due to the limited availability of data regarding their effects in adipocytes. Their adipogenic potential was assessed in SGBS cells using a lipid accumulation assay. Importantly, the nanomolar concentration range included in this study is within the range of reported human exposure levels. BPA has been detected in multiple human matrices, including serum (up to 6.5 ng/mL in pregnant Chinese women [48]), urine (mean 1.3 ng/mL in the US population [49]), and adipose tissue, where concentrations ranging from 1.8 to 12.01 ng/g tissue were reported in Spanish women [50]. In our experiment, all bisphenols except BPA showed a significant increase in lipid accumulation following bisphenol exposure in the absence of

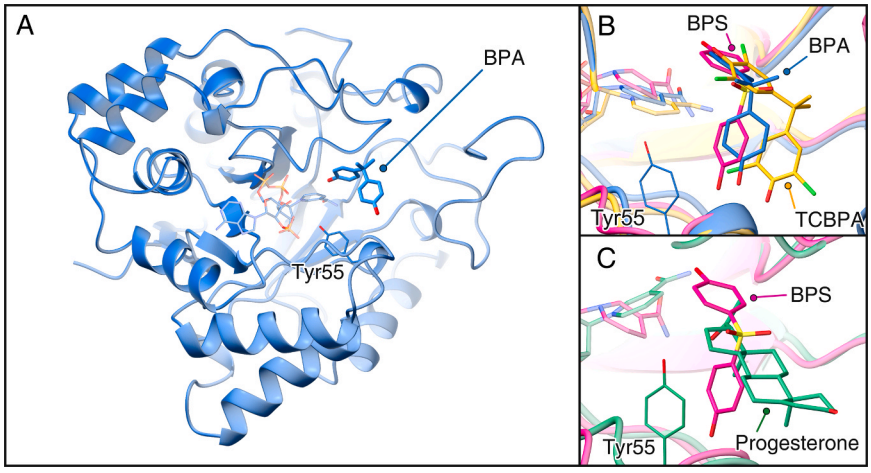

Fig. 8. MD-refined bisphenol binding poses in AKR1C1 derived from the 3C3U ternary template. (A) Overview of AKR1C1 with BPA and NADPH bound in the active site. (B) Common refined binding modes of BPA, BPS, and TCBPA in the steroid/inhibitor pocket. (C) Comparison of the refined BPS pose with progesterone in the same active-site region. Tyr55 is highlighted for orientation, and the cofactor is shown in the background.

PPARγ agonist rosiglitazone. Although BPA is widely recognized as a metabolism-disrupting chemical, its adipogenic effects are likely mediated through mechanisms distinct from those of the halogenated bisphenols. While brominated and chlorinated bisphenol derivatives directly activate PPARγ, BPA has been reported to exhibit weak or antagonistic activity towards this receptor [30,31]. Instead, BPA promotes the expression of genes involved in early adipogenesis, including PPARγ and other lipogenic genes, thereby indirectly facilitating adipocyte differentiation and adipocyte hypertrophy [32,33]. Consequently, the absence of a significant increase in lipid accumulation in the present study does not necessarily contradict the reported obesogenic properties of BPA but rather suggests a distinct mode of action.

Previous studies investigating the adipogenic effects of BPA have reported inconsistent findings. While most studies describe increased lipid accumulation following BPA exposure [73–76], others observed reduced lipid accumulation using SGBS cells in presence of rosiglitazone [31]. In contrast, BPS has consistently been reported to induce adipogenic effects that are comparable to or even stronger than those of BPA [23,76], which is in agreement with the findings of the present study. Furthermore, brominated BPA derivatives display a substantially higher affinity for PPARγ and directly activate the receptor [30], suggesting that halogenation fundamentally alters the receptor-binding properties of bisphenols and thereby enhances their adipogenic potential. Consistent with these findings, previous *in vitro* studies investigating TBBPA in 3T3-L1 mouse preadipocytes showed increased lipid accumulation and cell number, as well as a weak induction of mouse PPARγ [77]. Similarly, *in vivo* studies using zebrafish larvae demonstrated that TBBPA and TCBPA exert adipogenic effects, as indicated by increased lipid accumulation and the chemicals' capacity to induce zebrafish PPARγ [44].

PPARs are nuclear receptors, central for adipocyte biology and believed to be a key point of the adipogenic effect of metabolic disrupting chemicals [28,78,79]. PPARγ is specifically important for adipocyte differentiation, function and lipid metabolism [80,81] and is a target for a variety of endocrine-disrupting chemicals [30,31,82–84]. Schaffert et al. [31] showed an antagonistic effect for BPA and most tested analogues on this receptor, however, halogenated alternatives were not included in the analysis. In Riu et al. [30] the halogenated BPA alternatives showed an agonistic effect of TBBPA and TCBPA on human PPARγ. In the present study, BPS and its halogenated alternatives, TBBPS and TCBPS, all induced PPARγ activation. Contrary to Schaffert et al. [31], who reported an antagonistic effect of BPS on PPARγ using the GeneBLAzer assay, our results demonstrate weak agonistic activity of BPS in the HGLN reporter system, albeit with ~1000-fold lower potency than rosiglitazone. This discrepancy between studies can be explained by differences in assay design: while the HGLN system measures receptor activation in the absence of a competing ligand, the GeneBLAzer antagonism mode is performed in the presence of rosiglitazone, thereby assessing competitive interactions. Under these conditions, weak agonists by chemicals such as BPS can reduce the maximal activation induced by rosiglitazone, resulting in an apparent antagonistic effect. Thus, the previously reported antagonism of BPS may instead reflect weak partial agonism that interferes with full receptor activation by a high-affinity ligand. This, including the results in Riu et al. [30], where an increase of PPARγ activation was measured with increasing bromination-status of bisphenol A, shows, that the halogenation leads to a structural change, making the bisphenol a more potent activator for this nuclear receptor.

Crystal structure analyses indicate that BPA binds to the ligand-binding pocket (LBP) of PPARγ but does not interact with the key residue Y473 located on helix H12, and therefore fails to stabilize the receptor in its active conformation [85]. In contrast, other ligands such as the plasticizer monoisononylcyclohexane−1,2-dicarboxylic acid ester (MINCH) are able to stabilize helix H12 through direct interaction with Y473, resulting in stronger receptor activation [86]. Similarly, TBBPA and TCBPA do not exhibit direct stabilization of helix H12 [30]. However, Riu et al. [30] reported interactions between the halogen atoms of TBBPA and TCBPA and the PPARγ binding pocket. These interactions were proposed to contribute to receptor stabilization, potentially explaining their higher agonistic activity compared to BPA. Further structural studies are needed to analyze the binding modes of BPS-derived analogues such as TBBPS and TCBPS and their impact on PPARγ activation.

Quantification of adipokines after bisphenol exposure showed an increase in adiponectin secretion following 8-day exposure to BPS and its halogenated alternatives. Adiponectin is a PPARγ regulated gene and has anti-inflammatory as well as insulin sensitizing properties [66]. This increase may be an indicator of the interaction of these bisphenols with PPARγ. Contrary to our findings in mature adipocytes, Schaffert et al. [31] showed a slight decrease in adiponectin secretion after BPS exposure (12-day exposure during adipogenesis), suggesting a different impact of these chemicals on mature compared to differentiating adipocytes. MCP−1, an indicator for inflammatory processes and a chemokine for monocyte/macrophage infiltration/migration into tissues, varied over the course of exposure. Activation of PPARγ has also shown to decrease MCP−1 secretion [87]. Specifically following acute 24 h TCBPS exposure the MCP−1 secretion was significantly decreased but increased again after 4-day exposure, showing dynamic and changing effects. BPA exposure led to an increase in MCP−1 after 8 days, suggesting that these chemicals may exert similar effects in both mature and differentiating adipocytes, consistent with findings by Schaffert et al. [31], who reported increased MCP−1 secretion after BPA and BPS exposure during adipogenesis.

Analysis of proteome-level changes revealed similar pathway regulation in rosiglitazone-treated cells and cells exposed to TBBPS and TCBPS, particularly in pathways related to lipid and energy metabolism as well as cell structure. In addition to the established interaction of halogenated bisphenols with PPARγ [30,77], analysis of TBBPA also demonstrated an upregulation of genes associated with early stages of adipocyte differentiation, occurring prior to PPARγ activation [77]. Therefore, the adipogenic effects of TBBPA, and potentially, due to structural similarity, other halogenated bisphenols, are likely not solely driven by PPARγ activation but may also involve additional, yet unidentified mechanisms independent of PPARγ signaling.

Analysis of central carbon metabolites following bisphenol exposure revealed distinct alterations in cellular metabolite profiles. BPS and its halogenated derivatives exerted a strong increasing effect on glycolysis intermediates, with TCBPS showing the most pronounced impact. Consistent with this, BPS and its halogenated analogues increased overall levels of TCA cycle-associated metabolites, particularly acetyl-CoA and its derivative malonyl-CoA. Both metabolites serve as key substrates for fatty acid synthesis and thus represent an important metabolic link between glycolysis and TCA cycle [88]. These metabolite-level changes align with pathway-level observations, where halogenated BPS alternatives led to an upregulation of proteins associated with lipid and energy metabolism, including glycolysis/gluconeogenesis and the TCA cycle. Overall, the observed increase in lipid accumulation, the upregulation of lipid metabolism-associated pathways, and the elevated levels of metabolites linked to fatty acid synthesis and energy metabolism are consistent across experimental approaches. Together, these findings indicate a potential metabolism-disrupting effects of these novel bisphenol alternatives across multiple levels of analysis.

Our study unveiled novel targets of the tested bisphenols using TPP, which is a method that uses the biophysical properties of proteins and combines them with quantitative mass spectrometry-based proteomics [46]. The method follows the principle that the stability of a protein can be altered by its interactions [89]. We used this method to identify molecular targets of the bisphenols in the cell lysate of mature SGBS cells.

While TPP was originally developed for the identification of targets and off-targets of drug-like molecules [46], TPP is now also used for the analysis of interaction between proteins, metabolite binding, nucleic

acid-protein interactions and post-translational modifications [90]. More recently, TPP was applied to identify novel targets of MINCH in different stages of SGBS adipocyte differentiation [51].

The most relevant candidate proteins identified in this study clustered within functional categories related to fatty acid metabolism, steroid metabolism, and carbon and amino acid metabolism. These categories align well with the pathway alterations and changes in metabolites observed following bisphenol exposure in adipocytes.

The identified candidates not only showed functional clustering but also considerable overlap across the different bisphenol treatments, potentially due to structural similarities among the tested compounds. BPS and its halogenated alternatives induced the most pronounced shift with members of the AKR1C subfamily. These overlapping interactions of several bisphenols with members of the same enzyme subfamily, most prominently AKR1C1, indicate a shared enzyme-centered mode of interaction across structurally related compounds. The aldo-keto reductase C1 subfamily catalyzes the NAD(P)H-dependent conversion of aldehydes and ketones into their corresponding alcohols [91,92]. The strongest effects were observed on AKR1C1. AKR1C1 catalyzes the conversion of progesterone into its inactive metabolite, 20α-hydroxyprogesterone [92].

Studies found that all members of the ARK1C subfamily share a similar overall structure but show small differences in the catalytic site, leading to their distinct substrate specificity [92,93]. This specificity between the subtypes is largely determined by the structure of three large loops, which participate in substrate catalyst [92]. The cofactor binding domain is mostly identical between subtypes. Cofactor binding leads to a conformational change [94], which results in a mature substrate binding site. This was shown in the present study, as during nanoDSF, a stabilizing effect of the bisphenols was only observed in the presence of the protein's natural cofactor, NADPH, indicating that the interaction between AKR1C1 and the cofactor enables the binding of bisphenols or natural substrates. The inhibitor 3-bromo−5-phenylsalicylic acid had a similar stabilizing effect during nanoDSF to that of the tested bisphenols.

Crystal structure analysis of AKR1C1 and potent inhibitors like 3,5-dichlorosalicylic acid and 3-bromo−5-phenylsalicylic acid showed that these inhibitors bind the hydrophobic inhibitor binding pocket of AKR1C1 consists of a side chain, composed of 11 amino acids that lies within the enzymes catalytic domain [64,69].

AKR1C1 was selected for further validation because it displayed one of the largest and most significant thermal shifts in the TPP dataset, was identified as a target of multiple bisphenols, and belonged to the repeatedly enriched AKR1C enzyme family. In addition, the availability of well-characterized substrates and functional activity assays enabled orthogonal validation by nanoDSF and enzyme activity measurements. In our experimental setup, 3-bromo−5-phenylsalicylic acid led to a reduction of AKR1C1's normal enzymatic activity of about 35%. El-Kabbani et al. [69] found a K_i value of 4 nM for this particular inhibitor, therefore we expected a stronger inhibition at 10 μM. However, this result still serves as a reference point for enzyme inhibition in our setup. Interestingly, all tested bisphenols, except BPA and TBBPA, showed a stronger inhibitory effect on AKR1C1 than 3-bromo−5-phenylsalicylic acid. Our previous findings from TPP and nanoDSF demonstrated a general interaction between some of the tested bisphenols and AKR1C1. Beyond this, we were able to characterize the mechanistic basis of this interaction using both proteomics and enzyme activity assay, indicating that the interaction is most likely of inhibitory nature. Specifically, BPS and its halogenated alternatives had the strongest impact comparable to that of AKR1C1 inhibitor across multiple experimental settings. Taken together with the structural similarity between the halogenated bisphenols and the AKR1C1 inhibitor these findings suggest that bisphenols may interact with the inhibitory binding pocket within the catalytic substrate-binding site. This inhibition may have relevant downstream effects.

Through the reduction of progesterone into its inactive form, AKR1C1 regulates the availability of ligands for nuclear receptors (e.g. progesterone receptor) involved in steroid metabolism and thereby influences downstream transcriptional activities, including progesterone receptor signaling in progesterone-responsive tissues such as the uterus and breast tissue [95].

Adipose tissue is closely linked to peripheral sex steroid hormone metabolism [96], and progesterone has been shown to promote adipogenesis and exert lipogenic effects in adipocytes [97]. Within adipose tissue, AKR1C1 plays an important role in local progesterone metabolism by catalyzing the formation of 20α-hydroxyprogesterone [98,99]. Notably, AKR1C1 expression increases during adipocyte differentiation and has been associated with increased visceral fat mass in women, suggesting a link between AKR1C1 activity and adiposity [99,100]. Therefore, interactions of bisphenols with AKR1C1 may potentially affect adipocyte differentiation and adipose tissue homeostasis.

It should, however, be considered that the TPP experiment in this study was performed in cell lysates. While this approach is well suited to identify potential protein-compound interactions, it does not fully reflect intracellular target engagement under physiological conditions. Therefore, further studies are required to determine whether the investigated bisphenols interact with AKR1C1 in intact cells and to assess the resulting biological consequences (e.g. alterations in progesterone levels). Future applications of TPP in living cells could provide additional insight into these interactions under more physiological conditions.

Although the present study demonstrates that several bisphenols directly interact with and inhibit AKR1C1, it does not establish that AKR1C1 inhibition is causally responsible for the observed lipid accumulation and metabolic reprogramming. To strengthen the biological relevance of this interaction, future studies should quantify progesterone and 20α-hydroxyprogesterone following both bisphenol exposure and pharmacological AKR1C1 inhibition. Furthermore, genetic loss-of-function approaches, such as AKR1C1 knockdown or knockout in adipocytes, would be required to determine whether AKR1C1 inhibition is necessary for the observed metabolic phenotype. Finally, in vivo studies using genetic AKR1C1 models could investigate systemic consequences, including changes in body weight, adipose tissue morphology, and steroid hormone homeostasis.

The mode of action of BPA has been predominantly attributed to its estrogen-mimicking properties, enabling binding to estrogen receptors α and β and the subsequent disruption of estrogen receptor signaling, together with associated transcription factors and downstream pathways [13]. In this context, the identification of AKR1C1 as an interaction partner of several halogenated BPA alternatives could expand the spectrum of potential molecular targets of these compounds. Although the physiological relevance of this interaction remains to be established, the observed interaction with AKR1C1 could identify steroid and xenobiotic metabolism as a potential target of halogenated bisphenols, although whether this interaction contributes to the observed metabolic phenotype remains to be determined.

5. Conclusion

In summary, by combining phenotypic analysis, quantitative proteomics, targeted metabolomics, and thermal proteome profiling, this study identified adipocyte-associated effects of several halogenated BPA alternatives in an *in vitro* human SGBS adipocyte model. In particular, BPS and its halogenated analogues induced changes in lipid accumulation, adipokine secretion, protein pathway enrichment, and central carbon metabolite profile.

These effects are partly mediated through interference with PPARγ signaling but additionally involve previously unrecognized molecular targets, indicating that these compounds are questionable replacements for BPA/TBBPA. Beyond the established interaction with PPARγ, our data identified AKR1C1 as a novel target of bisphenols. TPP and nanoDSF consistently revealed interactions between multiple bisphenols

and AKR1C1. Together with the observed inhibition of AKR1C1 enzyme activity by the tested bisphenols, these findings suggest that AKR1C1-associated pathways may be a target of halogenated bisphenols. However, whether this interaction is causally involved in the observed metabolic phenotype remains to be established.

Collectively, the present findings expand the current understanding of potential molecular targets of (halogenated) bisphenols and highlight the value of combining receptor-based and proteomic as well as metabolomics approaches for the investigation of endocrine-active chemicals. Nevertheless, as the present study was conducted in an *in vitro* cell model, further validation in primary human adipocytes, more complex multicellular systems, and *in vivo* models is required to determine the physiological relevance of the identified mechanisms and their implications for human health risk assessment. Future replacement strategies for BPA should therefore incorporate evaluation of broader metabolic endpoints to prevent regrettable substitution.

Statement of significance

Bisphenol A (BPA), a widely used plastic monomer found in numerous consumer products, has been associated with endocrine and metabolic disruption, leading to increasing use of structurally related alternatives, including halogenated derivatives. However, the molecular mechanisms underlying the metabolic effects of these substitutes remain poorly understood. Using environmentally relevant concentrations of the most common halogenated bisphenol alternatives (TBBPA, TCBPA, TBBPS, and TCBPS) together with BPA and BPS in human adipocytes, we identified profound alterations in lipid, energy, and central carbon metabolism. Thermal proteome profiling revealed novel intracellular targets, including AKR1C1, whose interaction with BPS and halogenated analogues was characterized as functionally inhibitory. These findings provide novel mechanistic insight into metabolism-disrupting effects of emerging bisphenols and support more comprehensive, mechanism-informed risk assessment of BPA substitutes.

CRediT authorship contribution statement

Marina Grimaldi: Formal analysis. **Ulrike Rolle-Kampczyk:** Writing – review & editing, Conceptualization. **Maximilian Faissner:** Writing – review & editing, Visualization, Methodology, Formal analysis. **Jasmin Kleißen:** Writing – original draft, Visualization, Methodology, Formal analysis, Data curation, Conceptualization. **Patrick Balaguer:** Writing – review & editing, Formal analysis. **Martin Wabitsch:** Writing – review & editing, Resources. **Alix Sarah Aldehoff:** Writing – review & editing. **Christoph Flamm:** Writing – review & editing. **Cornelius Goerdeler:** Writing – review & editing. **Anna Didio:** Writing – review & editing, Formal analysis. **John Thomas Heiker:** Writing – review & editing, Supervision. **Isabel Karkossa:** Formal analysis. **Johannes Schmidt:** Writing – review & editing, Formal analysis. **Martin von Bergen:** Writing – review & editing, Supervision, Resources, Funding acquisition, Conceptualization. **Kristin Schubert:** Writing – review & editing, Supervision, Resources, Funding acquisition, Conceptualization. **Jörg Lehmann:** Writing – review & editing, Resources. **Stefan Kalkhof:** Writing – review & editing, Resources.

Declaration of Competing Interest

The authors declare that they have no known competing financial interests or personal relationships that could have appeared to influence the work reported in this paper.

Acknowledgments

The authors would like to thank Johanna Pfütze, Hans Fritsche, Maj Schuster and Nicole Bock for their qualified technical assistance with sample preparation and LC-MS/MS data acquisition. This work was carried out in the framework of the European Partnership for the Assessment of Risks from Chemicals (PARC) and has received funding from the European Union's Horizon Europe research and innovation programme under grant agreement no. 101057014. Views and opinions expressed are however those of the authors only and do not necessarily reflect those of the European Union or the Health and Digital Executive Agency. Neither the European Union nor the granting authority can be held responsible for them. K.S. is grateful for funding by the German Research Foundation (Project No. 530364326). MW received funding by the Federal Ministry of Research, Technology and Space (Bundesministerium für Forschung, Technologie und Raumfahrt, BMFTR) as part of the German Center for Child and Adolescent Health (DZKJ) under the funding code 01GL2407A. S.K. and J.L. received funding from the Fraunhofer Cluster of Excellence Immune-Mediated Diseases (CIMD_CED-AhR). M.F. and C.F. are funded by the Novo Nordisk Foundation (Grant NNF21OC0066551 'MATOMIC').

Appendix A. Supporting information

Supplementary data associated with this article can be found in the online version at doi:10.1016/j.jhazmat.2026.143238.

Data availability

The mass spectrometry proteomics data have been deposited to the ProteomeXchange Consortium via the PRIDE partner repository with the dataset identifier PXD077754 (TPP dataset) and PXD078145 (full proteome analysis). The metabolomics data is available at the NMDR website, the Metabolomics Workbench, https://www.metabolomicsworkbench.org where it has been assigned Study ID ST004842. The data can be accessed directly via its Project DOI: https://doi.org/10.21228/M8NK2D. This work is supported by NIH grant U2C-DK119886 and OT2-OD030544 grants.

References

[1] WHO. WHO European Regional Obesity Report 2022 2022 [24.04.2026]. Available from: https://www.who.int/europe/publications/i/item/9789289057738.
[2] Apovian, C.M., 2016. Obesity: Definition, Comorbidities, Causes, and Burden. Am J Manag Care 22 (7), 10.
[3] Heindel, J.J., Newbold, R., Schug, T.T., 2015. Endocrine disruptors and obesity. Nat Rev Endocrinol 11 (11), 653–661.
[4] Casals-Casas, C., Desvergne, B., 2011. Endocrine disruptors: from endocrine to metabolic disruption. Annu Rev Physiol 73, 135–162.
[5] Yilmaz, B., Terekeci, H., Sandal, S., Kelestimur, F., 2020. Endocrine disrupting chemicals: exposure, effects on human health, mechanism of action, models for testing and strategies for prevention. Rev Endocr Metab Disord 21 (1), 127–147.
[6] Martyniuk, C.J., Martinez, R., Navarro-Martin, L., Kamstra, J.H., Schwendt, A., Reynaud, S., Chalifour, L., 2022. Emerging concepts and opportunities for endocrine disruptor screening of the non-EATS modalities. Environ Res 204 (Pt A), 111904.
[7] Coelho, M., Oliveira, T., Fernandes, R., 2013. State of the art paper Biochemistry of adipose tissue: an endocrine organ. Arch Med Sci 2, 191–200.
[8] Biemann, R., Bluher, M., Isermann, B., 2021. Exposure to endocrine-disrupting compounds such as phthalates and bisphenol A is associated with an increased risk for obesity. Best Pract Res Clin Endocrinol Metab 35 (5), 101546.
[9] Vom Saal, F.S., Vandenberg, L.N., 2021. Update on the Health Effects of Bisphenol A: Overwhelming Evidence of Harm. Endocrinol 162 (3).
[10] ANSES. Annex XV Restriction Report Proposal For a Restriction; BPA M.R.C. ltd2014 [Available from: https://mcgroup.co.uk/news/20140214/pc-supply-reach-44-mln-tonnes.html.
[11] Bittner, G.D., Yang, C.Z., Stoner, M.A., 2014. Estrogenic chemicals often leach from BPA-free plastic products that are replacements for BPA-containing polycarbonate products. Environ Health 13 (1), 41.
[12] Savastano, S., Tarantino, G., D'Esposito, V., Passaretti, F., Cabaro, S., Liotti, A., Liguoro, D., Perruolo, G., Ariemma, F., Finelli, C., Beguinot, F., Formisano, P., Valentino, R., 2015. Bisphenol-A plasma levels are related to inflammatory markers, visceral obesity and insulin-resistance: a cross-sectional study on adult male population. J Transl Med 13, 169.
[13] Acconcia, F., Pallottini, V., Marino, M., 2015. Molecular Mechanisms of Action of BPA. Dose Response 13 (4), 1559325815610582.
[14] Do, M.T., Chang, V.C., Mendez, M.A., de Groh, M., 2017. Urinary bisphenol A and obesity in adults: results from the Canadian Health Measures Survey. Health Promot Chronic Dis Prev Can 37 (12), 403–412.

[15] Shankar, A., Teppala, S., 2011. Relationship between urinary bisphenol A levels and diabetes mellitus. J Clin Endocrinol Metab 96 (12), 3822–3826.
[16] Bi, J., Wang, F., Wei, Y., Zhang, Y., Jia, C., He, J., Yao, J., Zhang, Z., Li, Z., Li, P., He, M., 2022. Association of serum bisphenol A levels with incident overweight and obesity risk and the mediating effect of adiponectin. Chemosphere 308 (Pt 2), 136287.
[17] Junge, K.M., Leppert, B., Jahreis, S., Wissenbach, D.K., Feltens, R., Grutzmann, K., Thurmann, L., Bauer, T., Ishaque, N., Schick, M., Bewerunge-Hudler, M., Roder, S., Bauer, M., Schulz, A., Borte, M., Landgraf, K., Korner, A., Kiess, W., von Bergen, M., Stangl, G.I., Trump, S., Eils, R., Polte, T., Lehmann, I., 2018. MEST mediates the impact of prenatal bisphenol A exposure on long-term body weight development. Clin Epigenetics 10, 58.
[18] Provvisiero, D.P., Pivonello, C., Muscogiuri, G., Negri, M., de Angelis, C., Simeoli, C., Pivonello, R., Colao, A., 2016. Influence of Bisphenol A on Type 2 Diabetes Mellitus. Int J Environ Res Public Health 13 (10).
[19] Eid, J.I., Eissa, S.M., El-Ghor, A.A., 2015. Bisphenol A induces oxidative stress and DNA damage in hepatic tissue of female rat offspring. J Basic Appl Zool 71, 10–19.
[20] Veiga-Lopez, A., Pennathur, S., Kannan, K., Patisaul, H.B., Dolinoy, D.C., Zeng, L., Padmanabhan, V., 2015. Impact of Gestational Bisphenol A on Oxidative Stress and Free Fatty Acids: Human Association and Interspecies Animal Testing Studies. Endocrinology 156 (3), 911–922.
[21] Xin, F., Jiang, L., Liu, X., Geng, C., Wang, W., Zhong, L., Yang, G., Chen, M., 2014. Bisphenol A induces oxidative stress-associated DNA damage in INS-1 cells. Mutat Res/Genet Toxicol Environ Mutagen 769, 29–33.
[22] Nayak, D., Adiga, D., Khan, N.G., Rai, P.S., Dsouza, H.S., Chakrabarty, S., Gassman, N.R., Kabekkodu, S.P., 2022. Impact of Bisphenol A on Structure and Function of Mitochondria: A Critical Review. Rev Environ Contam Toxicol 260 (1), 10.
[23] Ahmed, S., Atlas, E., 2016. Bisphenol S- and bisphenol A-induced adipogenesis of murine preadipocytes occurs through direct peroxisome proliferator-activated receptor gamma activation. Int J Obes 40 (10), 1566–1573.
[24] Ahmed, F., Sarsenbayeva, A., Katsogiannos, P., Aguer, C., Pereira, M.J., 2020. The effects of bisphenol A and bisphenol S on adipokine expression and glucose metabolism in human adipose tissue. Toxicol 445, 152600.
[25] Hugo, E.R., Brandebourg, T.D., Woo, J.G., Loftus, J., Alexander, J.W., Ben-Jonathan, N., 2008. Bisphenol A at environmentally relevant doses inhibits adiponectin release from human adipose tissue explants and adipocytes. Environ Health Perspect 116 (12), 1642–1647.
[26] Menale, C., Piccolo, M.T., Cirillo, G., Calogero, R.A., Papparella, A., Mita, L., Del Giudice, E.M., Diano, N., Crispi, S., Mita, D.G., 2015. Bisphenol A effects on gene expression in adipocytes from children: association with metabolic disorders. J Mol Endocrinol 54 (3), 289–303.
[27] Ariemma, F., D'Esposito, V., Liguoro, D., Oriente, F., Cabaro, S., Liotti, A., Cimmino, I., Longo, M., Beguinot, F., Formisano, P., Valentino, R., 2016. Low-Dose Bisphenol-A Impairs Adipogenesis and Generates Dysfunctional 3T3-L1 Adipocytes. PLoS One 11 (3), e0150762.
[28] Tyagi, S., Gupta, P., Saini, A.S., Kaushal, C., Sharma, S., 2011. The peroxisome proliferator-activated receptor: A family of nuclear receptors role in various diseases. J Adv Pharm Technol Res 2 (4), 236–240.
[29] Flores Gomez, D., Korpel, N., Grimaldi, M., Carivenc, C., Balaguer, P., Bourguet, W., Kamstra, J.H., 2026. Mechanistic Insights of BPA Alternatives on PPARgamma Binding and the Consequence on Adipocyte Differentiation. Environ Sci Technol.
[30] Riu, A., Grimaldi, M., le Maire, A., Bey, G., Phillips, K., Boulahtouf, A., Perdu, E., Zalko, D., Bourguet, W., Balaguer, P., 2011. Peroxisome proliferator-activated receptor gamma is a target for halogenated analogs of bisphenol A. Environ Health Perspect 119 (9), 1227–1232.
[31] Schaffert, A., Krieg, L., Weiner, J., Schlichting, R., Ueberham, E., Karkossa, I., Bauer, M., Landgraf, K., Junge, K.M., Wabitsch, M., Lehmann, J., Escher, B.I., Zenclussen, A.C., Korner, A., Bluher, M., Heiker, J.T., von Bergen, M., Schubert, K., 2021. Alternatives for the worse: Molecular insights into adverse effects of bisphenol a and substitutes during human adipocyte differentiation. Environ Int 156, 106730.
[32] Somm, E., Schwitzgebel, V.M., Toulotte, A., Cederroth, C.R., Combescure, C., Nef, S., Aubert, M.L., Huppi, P.S., 2009. Perinatal exposure to bisphenol a alters early adipogenesis in the rat. Environ Health Perspect 117 (10), 1549–1555.
[33] Swedenborg, E., Rüegg, J., Mäkelä, S., Pongratz, I., 2009. Endocrine disruptive chemicals: mechanisms of action and involvement in metabolic disorders. J Mol Endocrinol 43 (1), 1–10.
[34] ECHA. Assessment of regulatory needs. 2021.
[35] Ivry Del Moral, L., Le Corre, L., Poirier, H., Niot, I., Truntzer, T., Merlin, J.F., Rouimi, P., Besnard, P., Rahmani, R., Chagnon, M.C., 2016. Obesogen effects after perinatal exposure of 4,4′-sulfonyldiphenol (Bisphenol S) in C57BL/6 mice. Toxicol 357-358, 11–20.
[36] EFSA, 2024. Update of the scientific opinion on tetrabromobisphenol A (TBBPA) and its derivatives in food. EFSA J 22 (7), e8859.
[37] Song, S., Li, Y., Lv, L., Dong, M., Qin, Z., 2024. Tetrabromobisphenol A exerts thyroid disrupting effects but has little overt impact on postnatal brain development and neurobehaviors in mice. J Environ Sci 142, 1–10.
[38] Xiong, Y.M., Li, Y.Y., Lv, L., Chen, X.Y., Li, X.H., Qin, Z.F., 2023. Postnatal exposure to low-dose tetrabromobisphenol A increases the susceptibility of mammal testes to chemical-induced spermatogenic stress in adulthood. Environ Int 171, 107683.
[39] Dufour, P., Pirard, C., Charlier, C., 2017. Determination of phenolic organohalogens in human serum from a Belgian population and assessment of parameters affecting the human contamination. Sci Total Environ 599-600, 1856–1866.
[40] Yang, Y., Lu, L., Zhang, J., Yang, Y., Wu, Y., Shao, B., 2014. Simultaneous determination of seven bisphenols in environmental water and solid samples by liquid chromatography–electrospray tandem mass spectrometry. J Chromatogr A 1328, 26–34.
[41] Qu, G., Liu, A., Hu, L., Liu, S., Shi, J., Jiang, G., 2016. Recent advances in the analysis of TBBPA/TBBPS, TBBPA/TBBPS derivatives and their transformation products. TrAC Trends Anal Chem 83, 14–24.
[42] Wang, X., Liu, J., Liu, A., Liu, Q., Du, X., Jiang, G., 2012. Preparation and evaluation of mesoporous cellular foams coating of solid-phase microextraction fibers by determination of tetrabromobisphenol A, tetrabromobisphenol S and related compounds. Anal Chim Acta 753, 1–7.
[43] Li, A., Zhuang, T., Shi, W., Liang, Y., Liao, C., Song, M., Jiang, G., 2020. Serum concentration of bisphenol analogues in pregnant women in China. Sci Total Environ 707, 136100.
[44] Riu, A., McCollum, C.W., Pinto, C.L., Grimaldi, M., Hillenweck, A., Perdu, E., Zalko, D., Bernard, L., Laudet, V., Balaguer, P., Bondesson, M., Gustafsson, J.A., 2014. Halogenated bisphenol-A analogs act as obesogens in zebrafish larvae (Danio rerio). Toxicol Sci 139 (1), 48–58.
[45] Yu, Y., Tian, J.-L., Zheng, T., Li, Z.-R., Hao, C.-J., Xiang, M.D., Li, Z.-C., 2024. Perturbation of lipid metabolism in 3T3-L1 at different stages of preadipocyte differentiation and new insights into the association between changed metabolites and adipogenesis promoted by TBBPA or TBBPS. J Hazard Mater 2024 (465).
[46] Savitski, M.M., Reinhard, F.B., Franken, H., Werner, T., Savitski, M.F., Eberhard, D., Molina, Martinez, Jafari, D., Dovega, R., Klaeger, R.B., Kuster, S., Nordlund, B., Bantscheff, P., Drewes, M., 2014. G. Tracking cancer drugs in living cells by thermal profiling of the proteome. Science 346 (6205), 1255784.
[47] Franken, H., Mathieson, T., Childs, D., Sweetman, G.M., Werner, T., Togel, I., Doce, C., Gade, S., Bantscheff, M., Drewes, G., Reinhard, F.B., Huber, W., Savitski, M.M., 2015. Thermal proteome profiling for unbiased identification of direct and indirect drug targets using multiplexed quantitative mass spectrometry. Nat Protoc 10 (10), 1567–1593.
[48] Yang, J., Wang, H., Du, H., Xu, L., Liu, S., Yi, J., Chen, Y., Jiang, Q., He, G., 2020. Serum Bisphenol A, glucose homeostasis, and gestational diabetes mellitus in Chinese pregnant women: a prospective study. Environ Sci Pollut Res 28 (10), 12546–12554.
[49] Liu, B., Lehmler, H.J., Sun, Y., Xu, G., Liu, Y., Zong, G., Sun, Q., Hu, F.B., Wallace, R.B., Bao, W., 2017. Bisphenol A substitutes and obesity in US adults: analysis of a population-based, cross-sectional study. Lancet Planet Health 1 (3), e114–e122.
[50] Fernández, M., Arrebola, J., Taoufiki, J., Navalón, A., Ballesteros, O., Pulgar, R., Vílchez, J., Olea, N., 2007. Bisphenol-A and chlorinated derivatives in adipose tissue of women. Reprod Toxicol 24, 259–264.
[51] Aldehoff, A.S., Karkossa, I., Broghammer, H., Krupka, S., Weiner, J., Goerdeler, C., Nuwayhid, R., Langer, S., Wabitsch, M., Rolle-Kampczyk, U., Kloting, N., Bluher, M., Heiker, J.T., von Bergen, M., Schubert, K., 2025. Advanced Proteomics Approaches Hold Potential for the Risk Assessment of Metabolism-Disrupting Chemicals as Omics-Based NAM: A Case Study Using the Phthalate Substitute DINCH. Environ Sci Technol 59 (31), 16193–16216.
[52] Goerdeler, C., Engelmann, B., Aldehoff, A.S., Schaffert, A., Bluher, M., Heiker, J. T., Wabitsch, M., Schubert, K., Rolle-Kampczyk, U., von Bergen, M., 2024. Metabolomics in human SGBS cells as new approach method for studying adipogenic effects: Analysis of the effects of DINCH and MINCH on central carbon metabolism. Environ Res 252 (Pt 2), 118847.
[53] Aldehoff, A.S., Karkossa, I., Goerdeler, C., Krieg, L., Schor, J., Engelmann, B., Wabitsch, M., Landgraf, K., Hackermuller, J., Korner, A., Rolle-Kampczyk, U., Schubert, K., von Bergen, M., 2024. Unveiling the dynamics of acetylation and phosphorylation in SGBS and 3T3-L1 adipogenesis. iScience 27 (6), 109711.
[54] Wabitsch, M., Brenner, R.E., Melzner, I., Braun, M., Möller, P., Heinze, E., Debatin, K.-M., Hauner, H., 2001. Characterization of a human preadipocyte cell strain with high capacity for adipose differentiation. Int J Obes 25, 8–15.
[55] Aldridge, A., Kouroupis, D., Churchman, S., English, A., Ingham, E., Jones, E., 2013. Assay validation for the assessment of adipogenesis of multipotential stromal cells–a direct comparison of four different methods. Cytotherapy 15 (1), 89–101.
[56] Seimandi, M., Lemaire, G., Pillon, A., Perrin, A., Carlavan, I., Voegel, J.J., Vignon, F., Nicolas, J.C., Balaguer, P., 2005. Differential responses of PPARalpha, PPARdelta, and PPARgamma reporter cell lines to selective PPAR synthetic ligands. Anal Biochem 344 (1), 8–15.
[57] Garoche, C., Boulahtouf, A., Grimaldi, M., Chiavarina, B., Toporova, L., den Broeder, M.J., Legler, J., Bourguet, W., Balaguer, P., 2021. Interspecies Differences in Activation of Peroxisome Proliferator-Activated Receptor gamma by Pharmaceutical and Environmental Chemicals. Environ Sci Technol 55 (24), 16489–16501.
[58] Karkossa I. proteomicsr: An analysis pipeline for label-based and label-free proteomics data. 1.4.3 ed2023.
[59] Buescher, J.M., Moco, S., Sauer, U., Zamboni, N., 2010. Ultrahigh Performance Liquid Chromatography−Tandem Mass Spectrometry Method for Fast and Robust Quantification of Anionic and Aromatic Metabolites. Anal Biochem 82 (11), 4403–4412.
[60] Mateus, A., Bobonis, J., Kurzawa, N., Stein, F., Helm, D., Hevler, J., Typas, A., Savitski, M.M., 2018. Thermal proteome profiling in bacteria: probing protein state in vivo. Mol Syst Biol 14 (7), MSB188242.

[61] Childs D., Kurzawa N., Franken H., Doce C., Savitski M., Huber W. Analyze thermal proteome profiling (TPP) experiments. 3.23.0 ed2024.
[62] Penning, T.M., Drury, J.E., 2007. Human aldo-keto reductases: Function, gene regulation, and single nucleotide polymorphisms. Arch Biochem Biophys 464 (2), 241–250.
[63] Couture, J.F., Legrand, P., Cantin, L., Luu-The, V., Labrie, F., Breton, R., 2003. Human 20alpha-hydroxysteroid dehydrogenase: crystallographic and site-directed mutagenesis studies lead to the identification of an alternative binding site for C21-steroids. J Mol Biol 331 (3), 593–604.
[64] Dhagat, U., Endo, S., Sumii, R., Hara, A., El-Kabbani, O., 2008. Selectivity Determinants of Inhibitor Binding to Human 20α-Hydroxysteroid Dehydrogenase: Crystal Structure of the Enzyme in Ternary Complex with Coenzyme and the Potent Inhibitor 3,5-Dichlorosalicylic Acid. J Med Chem 51 (15), 4844–4848.
[65] UniProt. Q04828 · AK1C1_HUMAN uniprot.org [Available from: https://www.uniprot.org/uniprotkb/Q04828/entry.
[66] Astapova, O., Leff, T., 2012. Adiponectin and PPARgamma: cooperative and interdependent actions of two key regulators of metabolism. Vitam Horm 90, 143–162.
[67] Zhang, Y., Chua Jr., S., 2017. Leptin Function and Regulation. Compr Physiol 8 (1), 351–369.
[68] Yadav, A., Saini, V., Arora, S., 2010. MCP-1: chemoattractant with a role beyond immunity: a review. Clin Chim Acta 411 (21-22), 1570–1579.
[69] El-Kabbani, O., Scammells, P.J., Gosling, J., Dhagat, U., Endo, S., Matsunaga, T., Soda, M., Hara, A., 2009. Structure-Guided Design, Synthesis, and Evaluation of Salicylic Acid-Based Inhibitors Targeting a Selectivity Pocket in the Active Site of Human 20α-Hydroxysteroid Dehydrogenase (AKR1C1). J Med Chem 52 (10), 3259–3264.
[70] Tanizawa, Y.N., K., Sasaki, T., Anno, T., Ohta, Y., Inoue, H., Matsuo, K., Koga, M., Furukawa, S., Oka, Y., 2002. Unregulated Elevation of Glutamate Dehydrogenase Activity Induces Glutamine-Stimulated Insulin Secretion, Identification and Characterization of a GLUD1 Gene Mutation and Insulin Secretion Studies With MIN6 Cells Overexpressing the Mutant Glutamate Dehydrogenase. Diabetes 51 (3), 712–717.
[71] Rochester, J.R., 2013. Bisphenol A and human health: a review of the literature. Reprod Toxicol 42, 132–155.
[72] Boucher, J.G., Ahmed, S., Atlas, E., 2016. Bisphenol S Induces Adipogenesis in Primary Human Preadipocytes From Female Donors. Endocrinol 157 (4), 1397–1407.
[73] Ohlstein, J.F., Strong, A.L., McLachlan, J.A., Gimble, J.M., Burow, M.E., Bunnell, B.A., 2014. Bisphenol a enhances adipogenic differentiation of human adipose stromal/stem cells. J Mol Endocrinol 53 (3), 345–353.
[74] Masuno, H., Iwanami, J., Kidani, T., Sakayama, K., Honda, K., 2005. Bisphenol A Accelerates Terminal Differentiation of 3T3-L1 Cells into Adipocytes through the Phosphatidylinositol 3-Kinase Pathway. Toxicol Sci 84 (2), 319–327.
[75] Héliès-Toussaint, C., Peyre, L., Costanzo, C., Chagnon, M.-C., Rahmani, R., 2014. Is bisphenol S a safe substitute for bisphenol A in terms of metabolic function? An in vitro study. Toxicol Appl Pharmacol 280 (2), 224–235.
[76] Martínez, M.Á., Blanco, J., Rovira, J., Kumar, V., Domingo, J.L., Schuhmacher, M., 2020. Bisphenol A analogues (BPS and BPF) present a greater obesogenic capacity in 3T3-L1 cell line. Food Chem Toxicol 140, 111298.
[77] Chappell, V.A., Janesick, A., Blumberg, B., Fenton, S.E., 2018. Tetrabromobisphenol-A Promotes Early Adipogenesis and Lipogenesis in 3T3-L1 Cells. Toxicol Sci 166 (2), 332–344.
[78] Desvergne, B., Wahli, W., 1999. Peroxisome proliferator-activated receptors - nuclear control of metabolism. Endocr Rev 20 (5), 649–688.
[79] Ozcagli, E., Kubickova, B., Jacobs, M.N., 2024. Addressing chemically-induced obesogenic metabolic disruption: selection of chemicals for in vitro human PPARalpha, PPARgamma transactivation, and adipogenesis test methods. Front Endocrinol 15, 1401120.
[80] Rosen, E.D., Sarraf, P., Troy, A.E., Bradwin, G., Moore, K., Milstone, D.S., Spiegelman, B.M., Mortensen, R.M., 1999. PPARγ Is Required for the Differentiation of Adipose Tissue In Vivo and In Vitro. Mol Cell 4 (4), 611–617.
[81] Lefterova, M.I., Haakonsson, A.K., Lazar, M.A., Mandrup, S., 2014. PPARgamma and the global map of adipogenesis and beyond. Trends Endocrinol Metab 25 (6), 293–302.
[82] Evans, N., Conley, J.M., Cardon, M., Hartig, P., Medlock-Kakaley, E., Gray Jr., L. E., 2022. vitro activity of a panel of per- and polyfluoroalkyl substances (PFAS), fatty acids, and pharmaceuticals in peroxisome proliferator-activated receptor (PPAR) alpha, PPAR gamma, and estrogen receptor assays. Toxicol Appl Pharmacol 449, 116136.
[83] Engel, A., Buhrke, T., Kasper, S., Behr, A.C., Braeuning, A., Jessel, S., Seidel, A., Volkel, W., Lampen, A., 2018. The urinary metabolites of DINCH((R)) have an impact on the activities of the human nuclear receptors ERalpha, ERbeta, AR, PPARalpha and PPARgamma. Toxicol Lett 287, 83–91.
[84] Schaffert, A., Karkossa, I., Ueberham, E., Schlichting, R., Walter, K., Arnold, J., Bluher, M., Heiker, J.T., Lehmann, J., Wabitsch, M., Escher, B.I., von Bergen, M., Schubert, K., 2022. Di-(2-ethylhexyl) phthalate substitutes accelerate human adipogenesis through PPARgamma activation and cause oxidative stress and impaired metabolic homeostasis in mature adipocytes. Environ Int 164, 107279.
[85] Useini, A., Schwerin, I.K., Kunze, G., Strater, N., 2024. Structural Studies on the Binding Mode of Bisphenols to PPARgamma. Biomol 14 (6).
[86] Useini, A., Engelberger, F., Kunze, G., Strater, N., 2023. Structural basis of the activation of PPARgamma by the plasticizer metabolites MEHP and MINCH. Environ Int 173, 107822.
[87] Foryst-Ludwig, A., Hartge, M., Clemenz, M., Sprang, C., Heß, K., Marx, N., Unger, T., Kintscher, U., 2010. PPARgamma activation attenuates T-lymphocyte-dependent inflammation of adipose tissue and development of insulin resistance in obese mice. Cardiovasc Diabetol 9 (1), 64.
[88] Wakil, S.J., Abu-Elheiga, L.A., 2009. Fatty acid metabolism: target for metabolic syndrome. J Lipid Res 50, S138–S143 (Suppl(Suppl)).
[89] Molina, D.M., Jafari, R., Ignatushchenko, M., Seki, T., Larsson, E.A., Dan, C., Sreekumar, L., Cao, Y., Nordlund, P., 2013. Monitoring Drug Target Engagement in Cells and Tissues Using the Cellular Thermal Shift Assay. Science 341 (6141), 84–87.
[90] Mateus, A., Kurzawa, N., Becher, I., Sridharan, S., Helm, D., Stein, F., Typas, A., Savitski, M.M., 2020. Thermal proteome profiling for interrogating protein interactions. Mol Syst Biol 16 (3), e9232.
[91] Penning, T.M., 2015. The aldo-keto reductases (AKRs): Overview. Chem Biol Interact 234, 236–246.
[92] Chu, X., He, S., Liu, Y., Liu, Y., Feng, F., Guo, Q., Zhao, L., Sun, H., 2022. Overview of human 20 alpha-hydroxysteroid dehydrogenase (AKR1C1): Functions, regulation, and structural insights of inhibitors. Chem Biol Interact 351, 109746.
[93] Byrns, M.C., Jin, Y., Penning, T.M., 2011. Inhibitors of type 5 17beta-hydroxysteroid dehydrogenase (AKR1C3): overview and structural insights. J Steroid Biochem Mol Biol 125 (1-2), 95–104.
[94] Penning, T.M., Jin, Y., Heredia, V.V., Lewis, M., 2003. Structure-function relationships in 3alpha-hydroxysteroid dehydrogenases: a comparison of the rat and human isoforms. J Steroid Biochem Mol Biol 85 (2-5), 247–255.
[95] Taraborrelli, S., 2015. Physiology, production and action of progesterone. Acta Obstet Gynecol Scand 94 (161), 8–16.
[96] Li, J., Papadopoulos, V., Vihma, V., 2015. Steroid biosynthesis in adipose tissue. Steroids 103, 89–104.
[97] Lacasa, D., Le Liepvre, X., Ferre, P., Dugail, I., 2001. Progesterone stimulates adipocyte determination and differentiation 1/sterol regulatory element-binding protein 1c gene expression. potential mechanism for the lipogenic effect of progesterone in adipose tissue. J Biol Chem 276 (15), 11512–11516.
[98] Blouin, K., Blanchette, S., Richard, C., Dupont, P., Luu-The, V., Tchernof, A., 2005. Expression and activity of steroid aldoketoreductases 1C in omental adipose tissue are positive correlates of adiposity in women. Am J Physiol Endocrinol Metab 288 (2), E398–E404.
[99] Zhang, Y., Nadeau, M., Faucher, F., Lescelleur, O., Biron, S., Daris, M., Rheaume, C., Luu-The, V., Tchernof, A., 2009. Progesterone metabolism in adipose cells. Mol Cell Endocrinol 298 (1-2), 76–83.
[100] Blanchette, S., Blouin, K., Richard, C., Dupont, P., Luu-The, V., Tchernof, A., 2005. Expression and activity of 20alpha-hydroxysteroid dehydrogenase (AKR1C1) in abdominal subcutaneous and omental adipose tissue in women. J Clin Endocrinol Metab 90 (1), 264–270.